Doctoral Thesis

The formation of electronically excited species in cell suspension

Marek Rác

Department of Biophysics

Centre of the Region Haná for Biotechnological and Agricultural Research

Faculty of Science, Palacký University

Olomouc, Czech Republic

Olomouc 2014

Bibliographical identification

Name of the author: Marek Rác

Title of the doctoral thesis: The formation of electronically excited species in cell suspension

Degree program field: Biophysics

Duration of Ph.D study: 2010-2015

Year of defense: 2015

Supervisor: Doc. RNDr. Pavel Pospíšil, Ph.D

Keywords: reactive oxygen species, oxidative stress, electronically excited species, lipid peroxidation, protein oxidation, DNA fragmentation, electron paramagnetic resosnance spectroscopy, photomultiplier tube, charged coupled device imaging

Content

Declaration I

I hereby declare that the Ph.D thesis is my original work and effort and that it has not been submitted anywhere for any award. I have written this thesis by myselve and where other information have been used, they have been acknowledged in the section „References".

Signature: …………………………...
Date and Place: …………………….…..

Declaration II

I hereby declare that this thesis is from the student's own work and effort and all other sources of information have been acknowledged in the section „References".

Signature: …………………………...
Date and Place: …………………….

List of Publications

Published:

I. Tiwari, A., Rac, M. & Pospíšil, P. Formation of superoxide anion and carbon-centered radicals by photosystem II under high light and heat stress-EPR spin-trapping study. *Journal of Bioenergetics and Biomembranes* **45**, 551-559, (2013).

II. Pospíšil, P., Prasad, A. & Rác, M. Role of reactive oxygen species in ultra-weak photon emission in biological systems. *Journal of Photochemistry and Photobiology B: Biology* (2014).

Accepted:

III. Rác M., Křupka M., Binder S., Sedlářová M., Matušková Z., Raška M. & Pospíšil P. Oxidative damage of U937 human leukemic cells caused by hydroxyl radical results in singlet oxygen formation, *PlosOne* (2015), DOI: 10.1371/journal.pone.0116958.

Submited

IV. Rác, M., Sedlářová M., & Pospíšil, P. The formation of electronically excited species in the human multiple myeloma cell suspension, *Scientific Reports*.

V. Pospíšil, P., Prasad, A. & Rác, M. Mechanism of the formation of electronically excited species by oxidative metabolic processes: Role of reactive oxygen species. *Journal of Photochemistry and Photobiology C*.

Acknowledgements

I would like to thank my supervisor Doc. RNDr. Pavel Pospíšil Ph.D. for guidance, support, and help during the whole time of my study. I would like to express my gratitude to Dr. Ankush Prasad and Dr. Anshu Rastogi for all the help and support they provided me. I would also like to thank to the rest of the department for creating a friendly environment and for providing me help and advice every time I needed.

Furthermore I would send my thanks to Prof. Sayuri Miyamoto and Prof. Paulo Di Mascio for allowing me to spend my internship in their laboratories, for their help and consultations.

Last but not least I would like to express my gratitude to my family and friends who were always there for me. This thesis would not be created without the support and encouragement from them.

INVESTMENTS IN EDUCATION DEVELOPMENT

Abbreviations

C	ground state chromophore
$^3C^*$	ecxited triplet chromophore
CCD	Charged coupled device
DABCO	1,4-diazabicyclo[2.2.2]octane
DNPH	2,4-dinitrophenylhydrazine
EDTA	ethylenediaminetetraacetic acid
EPR	electron paramagnetic resonance
FBS	fetal bovine serum
H_2O_2	hydrogen peroxide
$HO^•$	hydroxyl radical
HRP	horseradish peroxidase
MDA	malondialdehyde
$^1O_2$	singlet oxygen
$O_2^{•-}$	superoxide anion radical
PBS	phosphate buffer saline
PMT	photomultiplier tube
POBN	4-pyridyl-l-oxide-N-tert-butylnitrone
PVDF	polyvinllidene fluoride
ROS	reactive oxygen species
$R^•$	alkyl radical
$RO^•$	alkoxyl radical
$ROO^•$	peroxyl radical
ROH	hydroxide
ROOH	hydroperoxide
ROOR	1,2-Dioxetane
ROOOOR	tetroxide
R=O	ground state carbonyls
$^3(R=O)^*$	excited triplet carbonyl
SOSG	singlet oxygen sensor green
TEMPONE	2,2,6,6-tetramethyl-4-piperidone-1-oxyl
TMPD	2,2,6,6-tetramethyl-4piperidone

Abstract

In this thesis, the formation of electronically excited species in cell suspension exposed to reactive oxygen species was studied as well as the oxidative damage of biomolecules. In order to study the oxidative damage of lipids, proteins, and DNA, U937 cells were exposed to reactive oxygen species. Malondialdehyde was used as a marker of lipid peroxidation. Carbonyl groups were used for the detection of protein oxidation and DNA fragmentation was evaluated in order to study the oxidative damage to DNA. It is shown here that the lipid peroxidation was not initiated by the addition of hydrogen peroxide to the cell suspension, while the addition of Fenton reagent to the cell suspension resulted in the lipid peroxidation. The addition of both, hydrogen peroxide and Fenton reagent, resulted in the protein carbonylation with more pronounced effect after the addition of Fenton reagent and in the DNA fragmentation with non-significantly higher effect in the case of Fenton reagent. Two different electronically excited species were detected, triplet excited carbonyls and singlet oxygen. The detection of the triplet excited carbonyls formation from cell suspension containing U266 cells was performed using one-dimensional and two-dimensional ultra-weak photon emission. The formation of singlet oxygen from cell suspension containing U266 or U937 cells was detected by electron paramagnetic resonance, while the formation of singlet oxygen in both U266 and U937 cells was visualized by the confocal laser scanning microscopy. It is shown here that there is a correlation between the formation of triplet excited carbonyls and singlet oxygen in the cell suspension. Possible mechanisms for the biomolecules oxidation and electronically excited species formation are described in this thesis.

Introduction

Reactive oxygen species (ROS) are produced as a byproduct of either metabolic processes such as cellular respiration in mitochondria and photosynthesis in chloroplast [1-3] or oxidative burst in phagocytic cells known to play role in the defense against infection [4]. It is well known that ROS can be formed either by electron transport from highly reducing species to molecular oxygen or by excitation energy transfer from triplet chromophores to molecular oxygen [2]. Superoxide anion radical ($O_2^{\bullet-}$) is formed by the one-electron reduction of molecular oxygen (Scheme I, reaction 1) or by one-electron oxidation of hydrogen peroxide (H_2O_2). One-electron reduction of molecular oxygen catalyzed by NADPH oxidase during the respiratory burst in the phagocytic cells, xanthine oxidase in the cytoplasm and one-electron oxidation of H_2O_2 catalyzed by flavin oxidases in peroxisomes are other sources of $O_2^{\bullet-}$ in animal cells [5-7]. In plants, $O_2^{\bullet-}$ is formed by one-electron reduction of molecular oxygen by the stromal side of photosystem I [8] and photosystem II [9]. Hydrogen peroxide (H_2O_2) is formed by either one-electron reduction of $O_2^{\bullet-}$ (Scheme I, reaction 2) or by two-electron reduction of molecular oxygen. One-electron reduction of $O_2^{\bullet-}$ to H_2O_2 occurs either spontaneously or is catalyzed by superoxide dismutase located in the mitochondria, chloroplast and cytoplasm [10]. Two-electron reduction of molecular oxygen occurs during the reaction in which specific substrates are oxidized by the various types of oxidases in the mitochondria and peroxisomes [2, 11]. Hydroxyl radical ($HO^{\bullet}$) is formed by one-electron reduction of H_2O_2 catalyzed by metal in the reaction known as Fenton reaction [12] (Scheme I, reaction 3). Several types of metal ions such as iron, copper, manganese, zinc, chromium, cobalt, nickel and vanadium have been shown to reduce H_2O_2 to $HO^{\bullet}$. It is well known that metals are coordinated to active enzyme site in metalloproteins or stored in a ubiquitous protein called ferritin, hemosiderin, transferrin and lactoferrin [13, 14].
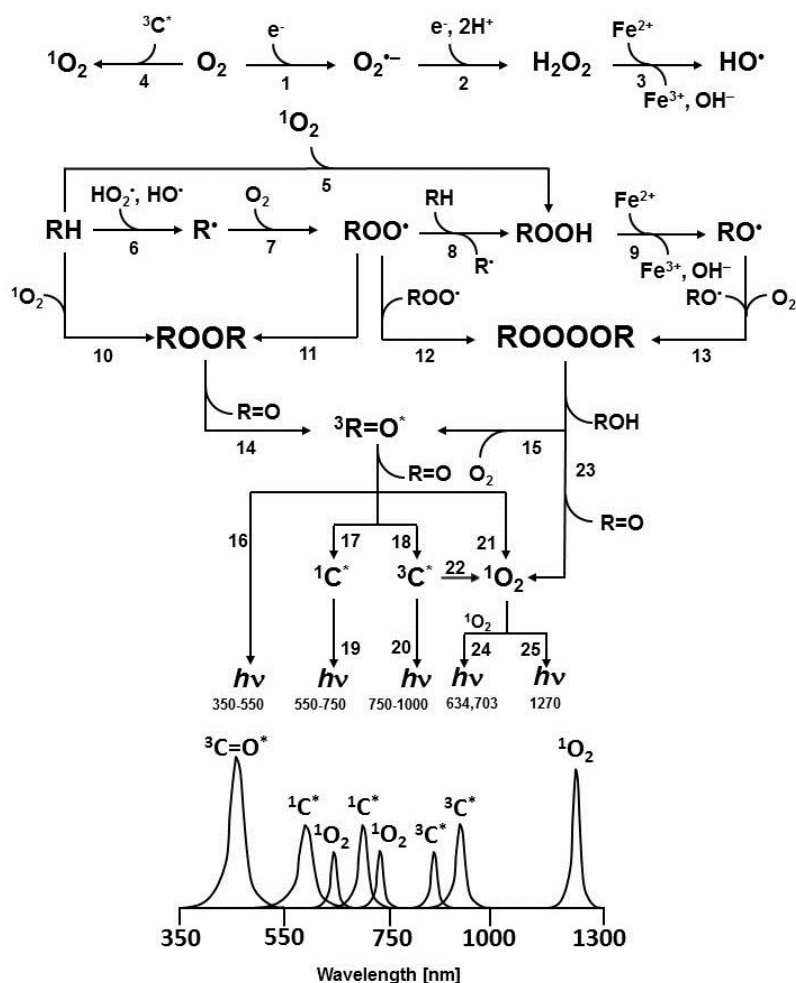
Scheme I: Mechanism of the formation of electronically excited species by oxidative metabolic processes

One-electron reduction of molecular oxygen by highly reducing species forms $O_2^{\bullet-}$ (reaction 1). The dismutation of $O_2^{\bullet-}$ generates H_2O_2 (reaction 2), whereas the subsequent one-electron reduction of H_2O_2 leads to the formation of $HO^{\bullet}$ (reaction 3). The triplet-triplet energy transfer from $^3C^*$ to molecular oxygen results in the formation of $^1O_2$ (reaction 4). Formation of ROOH from R and $^1O_2$ via ene reaction (5). The hydrogen abstraction from R by radical ROS ($HO^{\bullet}$, $HO_2^{\bullet}$) generates $R^{\bullet}$ (reaction 6). The subsequent one-electron oxidation of $R^{\bullet}$ brings about the formation $ROO^{\bullet}$ (reaction 7). The consequent hydrogen abstraction from another R by $ROO^{\bullet}$ forms ROOH (reaction 8). The one-electron reduction of ROOH results in the formation of $RO^{\bullet}$ and OH^- (reaction 9). ROOR is formed by either the cycloaddition of $^1O_2$ R (reaction 10) or the cyclization of $ROO^{\bullet}$ (reaction 11). ROOOOR is formed by the recombination of either two $ROO^{\bullet}$ (reaction 12) or hypothetically two $RO^{\bullet}$ (reaction 13). The decomposition of ROOR (reaction 14) or ROOOOR (reaction 15) results in the formation of $^3(R=O)^*$. The electronic transition from $^3(R=O)^*$ to R=O is accompanied by the photon emission (16). The energy transfer from $^3(R=O)^*$ to chromophores results in the formation of $^1C^*$ (reaction 17) and $^3C^*$ (reaction 18) chromophores. The electronic transition from $^1C^*$ and $^3C^*$ to the ground state of chromophore is accompanied by the photon emission. (reaction 19, 20). The triplet-triplet energy transfer from $^3(R=O)^*$ (reaction 21) and $^3C^*$ (reaction 22) to molecular oxygen forms $^1O_2$. Alternatively, the decomposition of ROOOOR via Russell-type mechanism, resulting in $^1O_2$ (reaction 23) with dimol photon emission (reaction 24) and monomol photon emission (reaction 25). (Paper V).

3

Singlet oxygen ($^1O_2$) is formed by triplet-singlet energy transfer from triplet excited chromophores ($^3C^*$) to molecular oxygen (Scheme I, reaction 4). To eliminate the oxidative damage of ROS, the non-enzymatic and enzymatic antioxidant systems are engaged. When ROS are not sufficiently eliminated by antioxidant defense systems, oxidative damage of biomolecules comprising lipid, protein and nucleic acid occurs [3, 15, 16].

Markers of oxidative damage

The formation of malondialdehyde (MDA), product of lipid peroxidation, is commonly used as a marker of oxidative damage of lipids [17]. Lipid peroxidation contains three steps: the initiation, propagation, and termination. The initiation starts with hydrogen abstraction from lipids mediated by HO$^{\bullet}$ resulting in the formation of lipid alkyl radical (R$^{\bullet}$) (Scheme II, panel A). Subsequently, the unstable lipid R$^{\bullet}$ reacts with molecular oxygen forming the lipid peroxyl radical (ROO$^{\bullet}$). During the propagation of lipid peroxidation, lipid ROO$^{\bullet}$ reacts with free fatty acid resulting in the formation of another radical. In the termination step, lipid ROO$^{\bullet}$ forms cyclic peroxide and subsequently cyclic endoperoxide [2] known to decompose to MDA [18]. Alternatively, the recombination of two lipid ROO$^{\bullet}$ leads to the formation of unstable tetroxide (ROOOOR) [19].

The protein carbonylation is commonly used as a marker of oxidative damage of proteins [20]. It is well established that the hydrogen abstraction from proteins by HO$^{\bullet}$ brings about the formation of protein R$^{\bullet}$ known to interact with molecular oxygen forming protein ROO$^{\bullet}$ (Scheme II, panel B). The second hydrogen abstraction by protein ROO$^{\bullet}$ from proteins leads to the formation of protein hydroperoxide (ROOH) known to be reduced to protein alkoxyl radical (RO$^{\bullet}$) by transition metals such as Fe^{2+}, Cu^+ and Zn^+. The β-scission of protein RO$^{\bullet}$

leads to the formation of protein carbonyls and protein R$^\bullet$ [21]. It has been assumed that the recombination of two protein ROO$^\bullet$ can result in the formation of ROOOOR [22].
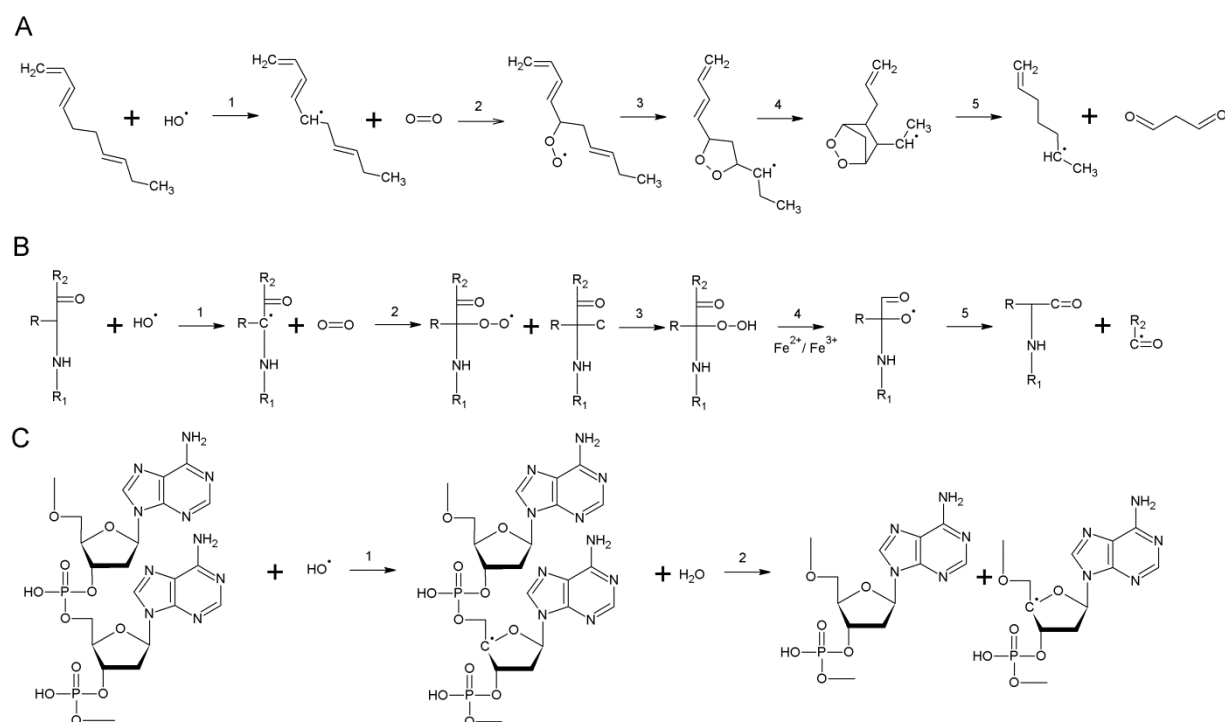
Scheme II. The formation of markers of oxidative damage

Panel A: Formation of MDA during lipid peroxidation. HO$^\bullet$ abstracts the hydrogen atom from lipid resulting in the formation of R$^\bullet$ (reaction 1). Subsequent reaction of R$^\bullet$ with molecular oxygen give raise to the ROO$^\bullet$ (reaction 2). ROO$^\bullet$ undergoes cyclization to form cyclic peroxide (reaction 3) and consequently cyclic endoperoxide (reaction 4) known to decompose to R$^\bullet$ and MDA (reaction 5). Panel B: Formation of protein carbonyl by β-scission of protein RO$^\bullet$. The abstraction of hydrogen from carbonyl by HO$^\bullet$ results in the formation of protein R$^\bullet$ (reaction 1) known to interact with molecular oxygen forming protein ROO$^\bullet$ (reaction 2). The second hydrogen abstraction by protein ROO$^\bullet$ leads to the formation of protein ROOH (reaction 3) known to be reduced to protein RO$^\bullet$ by Fe^{2+} (reaction 4). The β-scission of protein RO$^\bullet$ leads to the formation of protein carbonyls and protein alkyl radical (reaction 5). Panel C: DNA strand break initiated by HO$^\bullet$. Hydrogen abstraction from deoxyribose forms deoxyribose radical (reaction 1) resulting in the instability of the deoxyribose phosphate backbone leading to the strand break (reaction 2). (Paper III)

The DNA fragmentation is commonly used as a marker of oxidative damage of DNA [23]. It has been previously demonstrated that DNA fragmentation is initiated by the hydrogen abstraction by HO$^\bullet$ from deoxyribose forming deoxyribose radical (Scheme II,

panel C). The subsequent radical reactions of deoxyribose radical lead to the rearragement of the molecule of deoxyribose. The following scission of the deoxyribose phosphate backbone results in the formation of DNA strand breaks [24]. Alternativelly, the oxidative damage of DNA bases results in the alternation of the bases including thymine hydroperoxide. In the presence of metal ions or metalloproteins, thymine ROOH can be reduced to thyimine $ROO^\bullet$. The recombination of two thyimine $ROO^\bullet$ through the Russell mechanism results in the formation of unstable ROOOOR [25].

Formation of electronically excited species

The consequent reactions of organic radicals result in the formation of cyclic and linear high-energy intermediates. Cyclic high-energy intermediates are predominantly 1,2-dioxetanes (ROOR), whereas linear high-energy intermediates are ROOOOR [26, 27]. Several lines of evidence have shown that ROOR is formed either by the cycloaddition of $^1O_2$ to polyunsaturated fatty acids and amino acids (Scheme I, reaction 10) or by the cyclisation of $ROO^\bullet$ [28] (Scheme I, reaction 11). Tetroxides are formed by the recombination of two $ROO^\bullet$ [27] (Scheme I, reaction 12). The decomposition of ROOR and ROOOOR can lead to the formation of $^3(R{=}O)^*$. It has been shown that the excitation energy from $^3(R{=}O)^*$ can be transferred to molecular oxygen resulting in the formation of $^1O_2$ [29]. Beside the formation of $^3(R{=}O)^*$, ROOOOR decomposition can lead to the formation of $^1O_2$ via Russell mechanism [19].

1,2-Dioxetane

Scheme III shows in detail the formation of ROOR, either by the cycloaddition of $^1O_2$ to polyunsaturated fatty acids and amino acids (panel A) or by the cyclisation of $ROO^\bullet$ (panel B). The cycloaddition of $^1O_2$ to polyunsaturated fatty acids and amino acids results in the

formation of ROOR (Scheme IIIA, reaction 1) or endoperoxide (Scheme IIIA, reaction 2) [26, 28].
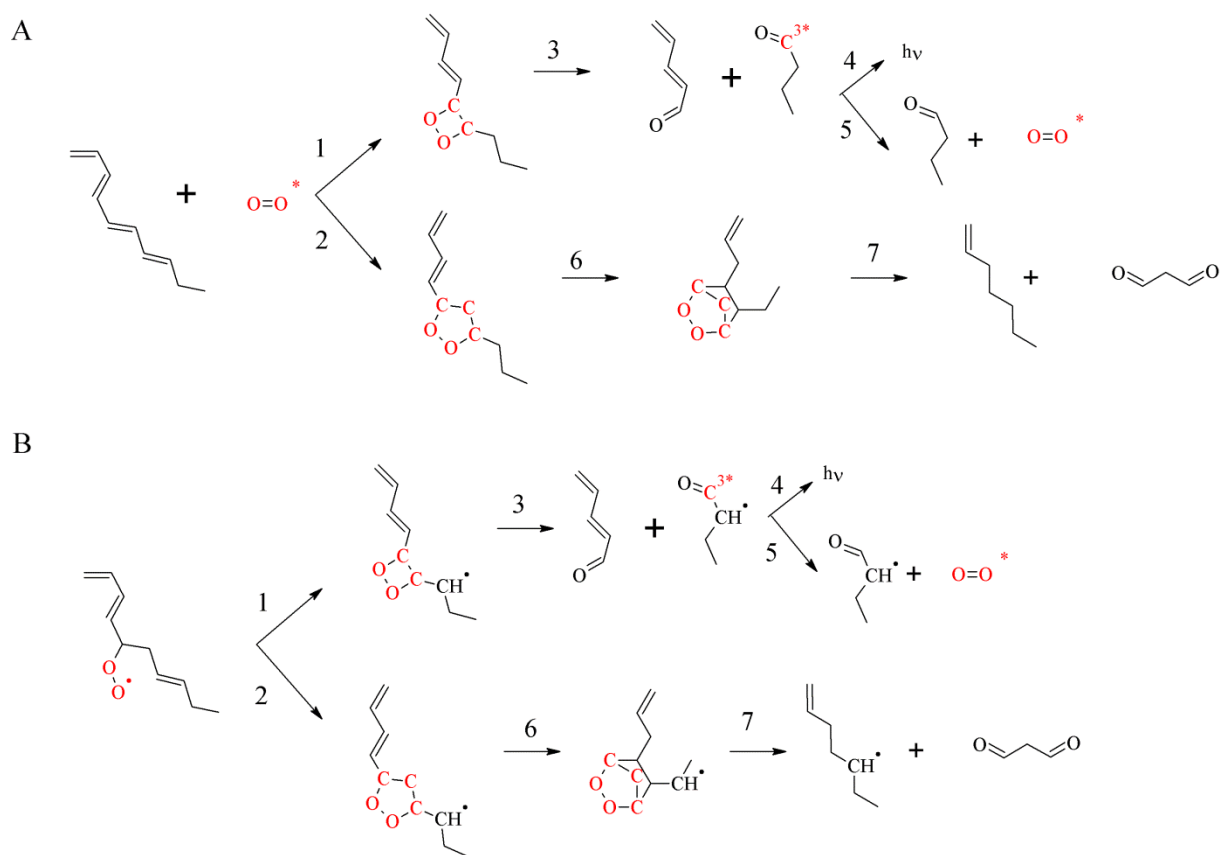
Scheme III: Formation of polyunsaturated fatty acid ROOR and endoperoxide by cycloaddition of $^1O_2$ to polyunsaturated fatty acid and amino acid (A) or by the cyclization of ROO$^•$(B)

In (A), the cycloaddition of $^1O_2$ to polyunsaturated fatty acid results in the formation of ROOR (reaction 1) or cyclic peroxide (reaction 2). 1,2-dioxetane is known to decompose into $^3(R=O)*$ and R=O (reaction 3). Subsequently, the electronic transition from triplet energy level of $^3(R=O)*$ to the ground energy level is associated with photon emission (reaction 4) or the energy transfer from $^3(R=O)*$ to molecular oxygen brings about the formation of $^1O_2$ (reaction 5). Cyclic peroxide can undergo structural change resulting in the formation of endoperoxide (reaction 6). The decomposition of endoperoxide gives a raise to polyunsaturated fatty acid and MDA (reaction 7). In (B), the cyclization of ROO$^•$ results in the formation of ROOR (reaction 1) or cyclic peroxide (reaction 2) both with R$^•$. 1,2-dioxetane is known to decompose into triplet excited carbonyl$^3(R=O)*$ with R$^•$ and R=O (reaction 3). Furthermore, the electronic transition from triplet energy level of $^3(R=O)*$ to the ground energy level is associated with photon emission (reaction 4) or the energy transfer from $^3(R=O)*$ to molecular oxygen brings about the formation of $^1O_2$ (reaction 5). Cyclic peroxide can undergo structural change resulting in the formation of endoperoxide with R$^•$ (reaction 6). The decomposition of endoperoxide gives a raise to R$^•$ and MDA (reaction 7). (Paper V)

The stereospecific [2+2] cycloaddition of $^1O_2$ has been shown to form ROOR consisting of two carbon atoms joined to two oxygen atoms, whereas stereospecific [4+2] cycloaddition of $^1O_2$ has been shown to generate endoperoxide consisting of four carbon atoms joined to two oxygen atoms [26, 30, 31]. Evidence has shown that ROOR is formed predominantly in an acidic environment via a protonated intermediate or in a nonpolar environment via an unprotonated intermediate [26]. It seems likely that at the membrane edge, ROOR is formed via protonated intermediate, while in the interior membrane, ROOR is formed via an unprotonated intermediate. Alternatively, the cyclisation of ROO$^\bullet$ has been shown to form ROOR containing R$^\bullet$ (Scheme IIIB, reaction 1). Subsequently, the R$^\bullet$ reaction with molecular oxygen, forming another ROO$^\bullet$, has been shown to result in the further cyclisation of ROO$^\bullet$ to produce bicyclic dioxetane [32]. Similar to the cycloaddition of $^1O_2$ to polyunsaturated fatty acids and amino acids, the cyclisation of ROO$^\bullet$ leads to the formation of endoperoxide (Scheme IIIB, reaction 2). Beside the ROS related formation of ROOR, there are also enzymatic reactions known to form ROOR [33, 34]. The decomposition of ROOR involves the cleavage of oxygen-oxygen and carbon-carbon bonds [35]. Two distinguishable mechanisms for the thermal decomposition of ROOR have been proposed [36]. The concerted mechanism involves the simultaneous cleavage of oxygen-oxygen and carbon-carbon bonds. The diradical mechanism is a two-step reaction involving the cleavage of oxygen-oxygen bond, resulting in the formation of diradical, followed by cleavage of the carbon-carbon bond [37].

Tetroxide

The oxidation of lipid, protein and DNA ROOH by metal ions, haemproteins, peroxynitrite, chloroperoxide and hypochlorous acid results in the formation of ROO$^\bullet$. Apart from a non-radical oxidant, RO$^\bullet$ has been proposed to be the cause of the oxidation of ROOH

to ROO•[25, 38]. The recombination of two ROO• initiates the formation of linear ROOOOR

via the Russell mechanism (Scheme IV, reaction 1) [19].
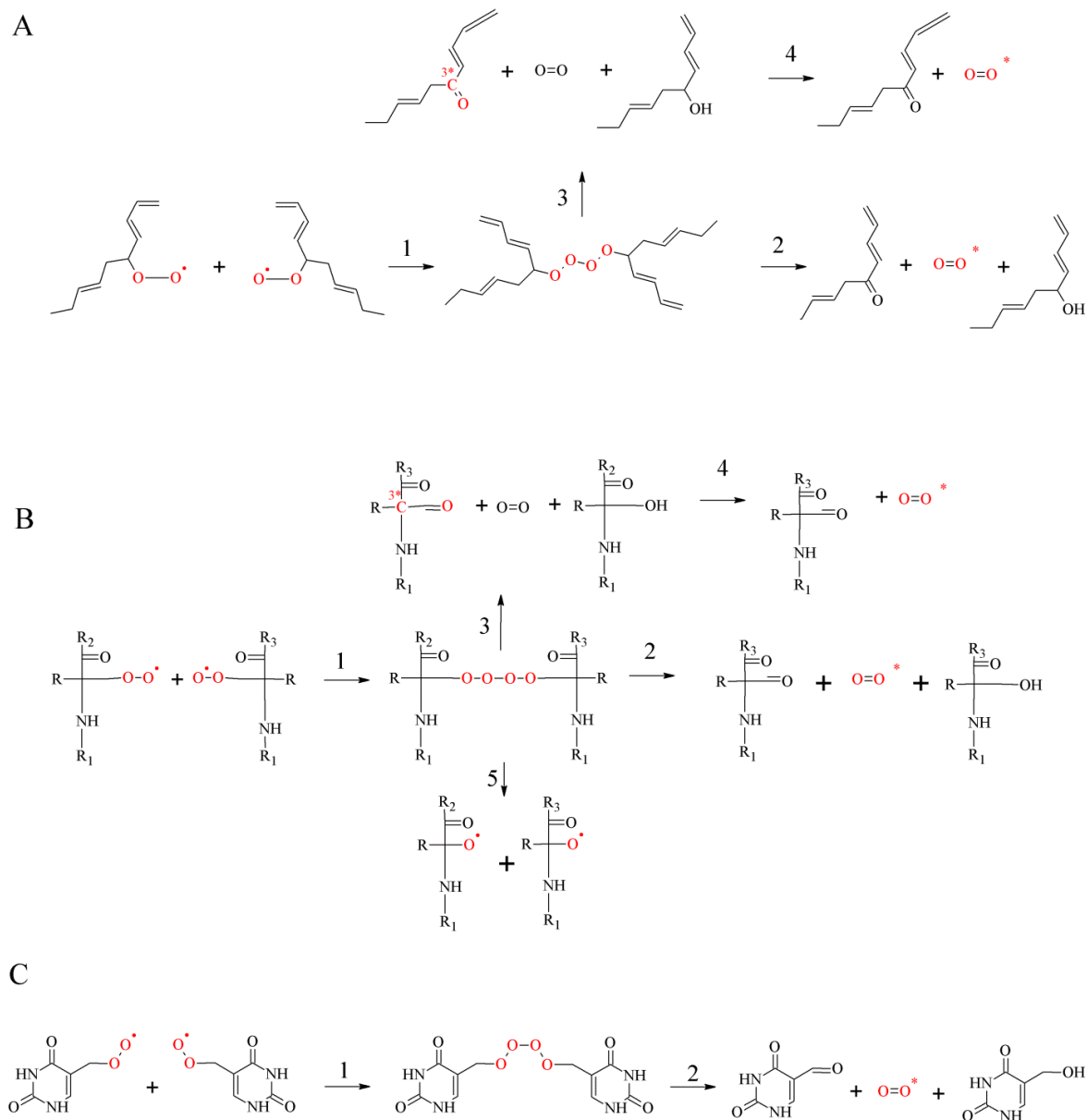
**Scheme IV: Formation of ROOOOR by recombination of two polyunsaturated fatty acid ROO• (A),
amino acid ROO• (B) and thymine ROO• (C)**

The recombination of two ROO• results in the formation of unstable ROOOOR (reaction 1). ROOOOR can
decompose into $^1O_2$, (R=O), and ROH (reaction 2). Alternatively, ROOOOR is known to decompose to ^{3}(R=O)*,
ROH and molecular oxygen (reaction 3). Subsequently, the electronic transition from ^{3}(R=O)* to the ground
energy level is associated with photon emission or the energy transfer from ^{3}(R=O)* to molecular oxygen
resulting in the $^1O_2$ formation (reaction 4). In the presence of reducing agents ROOOOR can decompose into 2
RO• (reaction 5). (Paper V)

It has been demonstrated that t-butyl hydroperoxide does not participate in the ROOOOR formation because the presence of α-hydrogen is required to undergo the Russell pathway [39, 40]. Based on this observation, it has been established that only the primary and secondary $ROO^\bullet$ are involved in the ROOOOR formation, while the tertiary $ROO^\bullet$ undergoes propagation of lipid peroxidation and protein oxidation.

Electronically excited states

The decomposition of high-energy intermediates ROOR (Scheme I, reaction 14) and ROOOOR (Scheme I, reaction 15) results in the formation of $^3(R{=}O)^*$ [41-43]. In the absence of chromophores or under anaerobic conditions, $^3(R{=}O)^*$ undergoes the electronic transition from the triplet excited state to the ground state accompanied by photon emission in the near UVA and blue-green regions of the spectrum (350-550 nm) [44, 45] (Scheme I, reaction 16). In the presence of chromophores, the excitation energy can be transferred from $^3(R{=}O)^*$ to choromophores [46] (Scheme I, reaction 17-18). The excited chromophores undergo the electronic transition from the excited state to the ground state accompanied by photon emission in the green-red (550-750 nm) (Scheme I, reaction 19) and the near IR (750-1000 nm) (Scheme I, reaction 20) depending on the type of chromophores [47]. Under aerobic conditions, the excitation energy can be transferred from $^3(R{=}O)^*$ to molecular oxygen [46] resulting in the formation of $^1O_2$ [29] (Scheme I, reaction 21). Apart from the formation of $^1O_2$ by triplet-singlet energy transfer from $^3(R{=}O)^*$ to molecular oxygen, $^1O_2$ is also formed by the decomposition of ROOOOR via Russell mechanism (Scheme I, reaction 23). It has been established that the recombination of $ROO^\bullet$ generates $^1O_2$ at a yield of 10% for most of the primary and secondary ROOOOR, while the formation of $^3(R{=}O)^*$ yields only 0.01% [48]. The Russell mechanism has been proven solely in the chemical system, and it is still unclear whether the Russell mechanism occurs also in the biological system [19, 40, 49, 50].

The role of electronically excited species in ultra-weak photon emission

In order to identify the role of electronically excited species in ultra-weak photon emission, two main approaches are used. The first one is the spectroscopic analysis of ultra-weak photon emission, while the second one is the usage of specific scavengers for individual electronically excited species. However, both mothods are accompanied with a lot of complications, therefore the results should have been considered carefuly. The downside of the spectroscopic analysis of ultra-weak photon emission is the very weak intensity, which makes the spectral analysis extremely hard, as well as the quantum efficiency of photomultiplier tubes (PMT). Usualy the quantum efficiency of PMTs varies from units to tens of percentages across the detected spectrum. Therefore proper recalculation of the detected spectra based on the quantum efficiency of PMT is required in order get the proper emission spectra. The application of specific scavengers can clearly confirm or exclude the involvement of electronically excited species in the ultra-weak photon emission detected. On the other hand, it is not possible to determine whether electronically excited species are involved in the chain reactions leading to the photon emission or the final emitter. Over the years, three main sources of ultra-weak photon emission were described: 1) $^3(R=O)^*$ in the near UVA and blue-green regions (350-550 nm), excited pigments in the green-red regions (550-700 nm) and 3) $^1O_2$ in the red (634 and 703 nm) and near IR (1270 nm) regions [51-54].

Triplet excited carbonyl

Spectral analysis of the ultra-weak photon emission from rat perfused lung induced by the addition of exogenous H_2O_2 showed that the photon emission is predominantly in the blue-green region of the spectrum [55] assiociated with $^3(R=O)^*$. Spectral analysis of the t-butyl hydroperoxide-induced ultra-weak photon emission from rats brain and liver homogenate showed small blue band between 410-440 nm [56]. The author suggested that the photon emission might be due to $^3(R=O)^*$ formed through the ROOR mechanism. The ultra-

weak emission from spinach mitochondria shows the photon emission in a wide spectral range from 450 nm to 750 nm [57]. The author proposed that $^3(R=O)^*$ contributes to the photon emission from 450 nm to 540 nm. Spectral analysis of the ultra-weak photon emission from the cotyledons of etiolated seedlings of *Cicer arietinum* L. subjected previously to the sudden freezing and thawing shows the photon emission in the spectral range from 390 nm to 440 nm, which correspond to the photon emission due to de-excitation of $^3(R=O)^*$ [58]. The ultra-weak photon emission from hemodialysis plasma cells after the addition of H_2O_2 and iron sulfate was found to be predominantly in the blue region of the spectrum with a peak at 430 nm likely attributed to $^3(R=O)^*$ [59]. The ultra-weak photon emission from low-molecular mass fraction obtained by HPLC-gel chromatography showed that the photon emission origins from molecules such as vitamin B_{12} and uric acid. It is proposed here that $HO^\bullet$ oxidized low-molecular-mass molecules to form ROOOOR know to decompose to $^3(R=O)^*$ as a final emitter. Spectral analysis of the ultra-weak photon emission from DNA treated with copper/ascorbate/H_2O_2 system showed that the photon emission is from 390 to 430 nm [60]. These results showed that $^3(R=O)^*$ formed through the ROOR mechanism is responsible for photon emission. Using a rotating wheel with a set of short wavelength sharp cut-off glass filters, Tadeka et al. [61] demonstrated that the ultra-weak photon emission from esophageal carcinoma cell line (TE9) is attributed to the photon emission of $^3(R=O)^*$ at around 450 nm [61]. Spectral analysis of elicitor-induced photon emission showed that photons are emitted in the blue-green region of the spectra (440-580 nm) [62]. Spectral analysis of ultra-weak photon emission measured after the topical application of H_2O_2 and organic peroxide (benzoylperoxide) to the porcine ex-vivo skin model showed that the photon emission is predominantly in the blue region of the spektra [63]. Similarly, the spectral analysis of ultra-weak photon emission measured after the addition of Fenton reagent (H_2O_2 and Fe^{2+}) to pure amino acid showed that Trp and Cys exhibit comparable photon emission in the broad

spectral ranges 420-550 nm, whereas His provides pronounced photon emission in the spectral range 420-455 nm. When ultra-weak photon emission was measured simultaneously from His to Trp, the photon emission in the spectral range 420-455 nm was suppressed. Based on this observation, the authors proposed that His transfers an excitation energy to Trp.

Singlet oxygen

Ultra-weak photon emission induced by the addition of exogenous organic peroxides (cumene hydroperoxide, ethyl hydroperoxide, t-butyl hydroperoxide) to cytochrome c was observed to be pronouncedly suppressed by $^1O_2$ scavengers such as β-carotene, His and Trp [64]. Contrary, the addition of $^1O_2$ dimol photon emission enhancer DABCO to cytochrome c treated with exogenous organic peroxides caused an enhancement in ultra-weak photon emission. Based on these observations, the authors proposed that dimol photon emission of $^1O_2$ is responsible for ultra-weak photon emission. The spectral analysis of photon emission from cytochrome c/H_2O_2 and cytochrome c/t-butyl hydroperoxide systems showed that the maximum photon emission from cytochrome c/H_2O_2 system is at 600-612 nm, whereas the maximum photon emission from cytochrome c/t-butyl hydroperoxide system is shifted toward longer wavelength range of 662-670 nm [64]. The authors proposed that in the cytochrome c/H_2O_2 system $^1O_2$ dimol photon emission at 634 nm is predominated, where in the cytochrome c/t-butyl hydroperoxide system $^1O_2$ dimol photon emission at 703 nm mainly contributes to the overall photon emission in the red region of the spectrum. These proposals have been confirmed by the spectral analysis of the ultra-weak photon emission from rat perfused lung induced by the addition of exogenous organic peroxides such as t-butyl hydroperoxide showing that the photon emission is mainly in the red region of the spectrum [52]. These observations indicate that the photon emission is predominantly due to $^1O_2$ dimol emission. The correlation between succinate-induced ultra-weak photon emission in the spinach mitochondria and formation of $^1O_2$ as detected by the bleaching of p-

nitrosodimethylaniline at 440 nm revealed the involvement of $^1O_2$ in ultra-weak photon emission [57]. Furthermore, succinate-induced ultra-weak photon emission was suppressed by $^1O_2$ scavenger such as sodium azide and enhanced by the $^1O_2$ dimol photon emission enhancer DABCO. These proposals were confirmed by the observation that succinate-induced ultra-weak photon emission in the spinach mitochondria appears predominantly at red region of the spectrum. The observation that the addition of a scavenger for $^1O_2$ such as 2,5-dimethyl furan suppressed significantly ultra-weak photon emission from the cotyledons of etiolated seedlings of *Cicer arietinum* L. subjected previously to the sudden freezing and thawing reveals that $^1O_2$ is a major source of ultra-weak photon emission [65]. Spectral analysis of the ultra-weak photon emission showed that the photon emission band in the range of 620-710 nm corresponds to the spectral range of the dimol emission from $^1O_2$. Agatsuma et al. [59] demonstrated that the addition of H_2O_2 to the healthy and hemodialysis plasma cells results in the ultra-weak photon emission predominantly in the red region of the spectrum with a peak at 680 nm. The ultra-weak photon emission from high-molecular-mass fraction obtained by HPLC-gel chromatography showed that the photon emission origins from proteins such as immunoglobin, albumin, cytochrome and microglobulin. It is proposed here that H_2O_2 oxidized proteins to form ROOOOR know to decompose to $^1O_2$ as a final emitter. The ultra-weak photon emission from esophageal carcinoma cell line (TE9) at around 580 nm, 634 nm and 703 nm is attributed to the photon emission from $^1O_2$ [61]. The detection of $^1O_2$ monomol photon emission at 1270 nm from lipid or thymine ROOH in the presence of redox active compounds confirmed the role of $^1O_2$ as the emitter of ultra-weak photon emission [25, 66].

Materials and methods

Cell cultures

Human leukemic monocyte lymphoma cell line U937 and human multiple myeloma cell line U266 were used for the experiments. Both cell cultures were grown in RPMI-1640 supplemented with 2 mM L-glutamine, 10% FBS, antibiotics at 37 °C in humidified 5% CO_2 atmosphere.

HPLC analysis

The sample preparation and derivatization of MDA with 2,4-dinitrophenylhydrazine (DNPH) was performed as described previously [67] with some modifications. Cell suspension containing U937 cells was treated with 5 mM H_2O_2 or Fenton reagent (5 mM H_2O_2 and 1 mM $FeSO_4$) for 30 min, centrifuged for 20 min at 11000 x g afterwards and supernatant was removed. Pellet was stirred up in 200 µl of phosphate buffer saline (PBS). After this, cells were disrupted by sonification for 90 s. The sample with disrupted cells was centrifuged at 2000 g for 10 min. The amount of 125 µl of supernatant was taken into the eppendorf vial and 25 µl of 6 M aqueous sodium hydroxide was added. This mixture was incubated in a 60 °C water bath for 30 min to achieve alkaline hydrolysis of protein bound MDA. Then, proteins were precipitated adding 62.5 µl of 35% (v/v) perchloric acid. The sample was vortexed and centrifuged at 16000 g for 10 min. A volume of 125 µl of supernatant was put into the dark eppendorf vial and mixed with 1 µl of 50 mM DNPH 50 % sulphuric acid. Subsequently, the mixture was incubated in dark for 30 min at room temperature. An aliquot of 50 µl of this mixture was injected into the HPLC system. The samples were analyzed on the HPLC system (Shimadzu LC-20A Prominence, Kyoto, Japan) with UV detection at 310 nm. A Lichrospher 100 RP-18 column (4.0 x 250 mm) with 5 µm particle size (Merck, Germany) preceded by a Lichrospher precolumn of the same material as

15

the stationary phase (4.0 x 4.0 mm) was used. Elution was performed isocraticaly with a mixture of 25 mM triethylamine adjusted to pH 3.5 and acetonitrile (50:50, v/v) at a flow rate of 1.5 ml/min at 35 °C.

Dot blot immunoassay

Proteins were isolated according to Pierce protocol with using RIPA buffer. Cell suspension containing U937 cells was treated with 5 mM H_2O_2 or Fenton reagent (5 mM H_2O_2 and 1 mM $FeSO_4$) for 30 min. Cells were washed twice in cold PBS. Cold RIPA buffer was added and mixture was incubated on ice for 5 min. Lysate was centrifuged at 14 000 x g for 15 min at 4°C. Supernatant containing proteins was derivatized with 400 μM DNPH for 30 min. Samples were transferred onto the PVDF membrane, using Don-blot apparatus (BioRad). Membrane was blocked in SuperBlock blocking buffer (Thermo Scientific) for 1 h and afterwards was incubated with primary antibody (anti-dinitrophenyl-KLH, rabbit IgG fraction, biotin-labeled, Molecular Probes) overnight. Than membrane was washed PBS-T buffer (PBS + Tween 20) and incubated with streptavidin-HRP conjugate in blocking buffer for 1 h. After washing, the reaction was visualized by electrochemiluminescence chemistry using X-ray sensitive film.

Comet Assay

Microscope slides were firstly precoated with 1% high melting point agarose (SERVA Electrophoresis), in distilled H_2O and then placed in a drying oven at temperature of 60 °C for at least 30 min. 85 μl of 1% high melting point agarose in PBS was applied on the precoated slides covered with a cover slip. The slides were then placed in a refrigerator in order to enhance gelling of the agarose. Cell suspension containing U937 cells treated with 5 mM H_2O_2 or Fenton reagent (5 mM H_2O_2 and 1 mM $FeSO_4$) for 30 min was centrifuged (6 min, 1200 rpm) and cell pellet was dispersed in 20 μl of PBS and vortexed. 85 μl of 1% low

melting point agarose was added into this solution and 85 μl of this suspension was cast on the solidified agarose on the microscope slide (the cover slide was removed prior to cell inoculation on the gel) and covered by a new glass cover slip to form a thin layer and moved to the refrigerator again. After solidifying the cover slips were removed again and the microscope slides were immersed in a lysis buffer (2.5 M NaCl), 100 mM EDTA, 10 mM Tris, 1% Triton X-100 (SERVA Electrophoresis), pH = 10) at 4 °C for at least 1 h. After the lysis the slides were washed in distilled water to remove all salts and then placed in an electrophoretic tank and dipped in cool electrophoresis solution (300 mM NaOH, 1 mM EDTA) for 40 min. Electrophoresis was run at 0.8 V/cm and 350 mA for 20 min. After the electrophoresis, the slides were rinsed 3x for 5 min with neutralisation buffer (0.4 M Tris, pH = 7.5) at 4 °C. The samples were subsequently stained by SYBR Green (Invitrogen). Fifty randomly chosen cells from each sample was visualized using fluorescence microscope Olympus IX 70 with CCD camera. Computerized image analysis system (TriTek CometScore™ Freeware 1.5) was used to measure several comet parameters (tail length, tail moment, tail % DNA).

EPR spin-trapping spectroscopy

EPR spin-trapping spectroscopy was used to monitor formation of $HO^\bullet$ in cell suspension containing U937 cell culture and $^1O_2$ in cell suspension containing U937 or U266 cell culture, respectively. Hydroxyl radical was detected by a 4-pyridyl-1-oxide-*N-tert*-butylnitrone (POBN)/ethanol spin-trapping system [68]. Cell suspension containing U937 cells was treated with 5 mM H_2O_2 or Fenton reagent (5 mM H_2O_2 and 1 mM $FeSO_4$) in the presence of 50 mM POBN, 170 mM ethanol, and culture medium. Singlet oxygen was detected by hydrophilic spin trap compound TMPD (2, 2, 6, 6-Tetramethyl-4-piperidone) [69]. To eliminate impurity TMPD EPR signal, TMPD was purified twice by vacuum

distillation. Cell suspensions were treated with 5 mM H_2O_2 or Fenton reagent (5 mM H_2O_2 and 1 mM $FeSO_4$) in the presence of 50 mM TMPD. Cell suspensions previously exposed to H_2O_2 and Fenton reagent treatments were put in a glass capillary tube (Blaubrand[®] intraMARK, Brand, Germany) and EPR spectra were recorded using an EPR spectrometer MiniScope MS400 (Magnettech GmbH, Berlin, Germany). EPR conditions were as follows: microwave power, 10 mW; modulation amplitude, 1 G; modulation frequency, 100 kHz; sweep width, 100 G; scan rate, 1.62 G s-1, gain 500. To prevent overscaling of EPR signal, the gain was decreased to 100, when EPR signal was measured 30 min after the addition of Fenton reagent to U937 cells. Simulation of EPR spectra was done using Winsim software freely available from the website of National Institute of Environmental Health Sciences.

Confocal laser scanning microscopy and image analysis

Singlet Oxygen Sensor Green (SOSG) reagent (Molecular Probes Inc. Eugene, OR, USA) was applied to the cell suspensions in order to visualize $^1O_2$ production. 5 mM SOSG stock solution was freshly prepared each time by adding 33 µl methanol to a 100 µg vial, and kept in darkness at 4 °C until used during a half-day work session. Studied cells were stained with the final concentration of 50 µM SOSG for 30 min, in darkness, at room temperature. Following incubation, the cells were gently washed with 20 mM K-buffer, and consequently the SOSG fluorescence was measured by confocal laser scanning microscope, Fluorview 1000 confocal unit attached to IX 80 inverted microscope (Olympus Czech Group, Prague, Czech Republic). Microphotographs were taken in the transmitted light detection module (405 nm excitation and Nomarski DIC filters) combined with the fluorescence channel, representing the SOSG fluorescence (excitation by a 488 nm line of argon laser and detection by 505-525 nm emission filter set). At the start of each experiment, the proper intensity of lasers was checked according to an unstained sample. To evaluate differential SOSG

fluorescence in individual experiments, the intensities of SOSG fluorescence within confocal images were analyzed using Olympus FV10-ASW 3.0 Viewer software. The average intensity of SOSG fluorescence superior to the background was calculated from the SOSG fluorescence channel of five to ten representative microphotographs per variant. The SOSG fluorescence within multiple layers of the cells was visualized with the vertical step of 0.5 µm.

Detection of ultra-weak photon emission

Ultra-weak photon emission was detected by PMT system installed in a black painted inner darkroom. The measurement systems inside the inner darkroom were controlled and data were recorded with the computer located in the outer darkroom. A low-noice PMT R7518P, sensitive in the spectral range 185 to 730 nm, and a photon counting unit C9744 (Hamamatsu Photonics K.K., Iwata City, Japan) were employed to measure one-dimensional photon emission. To reduce the dark noise, PMT was cooled down to -30 °C using thermoelectric cooler C9143 (Hamamatsu Photonics, K.K., Iwata City, Japan). All the measurements were recorded at -960 mV. The PMT was placed 5 cm above the sample during the measurement. In order to cut off the blue-green region of the spectra, long-pass edge interference filter (600 nm, Andover Corporation) was used.

Ultra-weak photon emission was visualised by CCD camera installed in a temperature controlled black box placed in a black painted inner darkroom. The measurement systems inside the inner darkroom were controlled and data were recorded with the computer located in the outer darkroom. The highly sensitive CCD camera VersArray 1300B (Princeton instruments, Trenton, NJ, USA) with spectral sensitivity in the range 350 to 1000 nm and close to 90% quantum efficiency in the visible range of the spectra was used to record the 2-D spectra. Objective lens of 50 mm focal distance (F mount Nikkor 50-mm, f:1,2, Nikon) was

used to enhance the light collecting efficiency. The CCD element was cooled down to -110°C in order to reduce the dark count. The following parameters were used during the measurement: scan rate 100 kHz; gain 2; image format 1340x1300 pixels; binning mode 4; distance between detector and the reflecting mirror 40 cm; and accumulation time 30 min.

Results

Formation of hydroxyl radical

To study the oxidative damage of biomolecules caused by $HO^\bullet$, H_2O_2 and Fenton reagent (H_2O_2 and $FeSO_4$) were added to cell suspension containing U937 cells. To confirm the formation of $HO^\bullet$ in the cell suspension after the addition of H_2O_2 and Fenton reagent, EPR spin-trapping spectroscopy was used. The detection of $HO^\bullet$ was accomplished using POBN/ethanol spin-trapping system. It is well established that the interaction of $HO^\bullet$ with ethanol yields α-hydroxyethyl radical ($CH(CH_3)HO^\bullet$) known to form a stable α-hydroxyethyl radical adduct of POBN (POBN-$CH(CH_3)OH$ adduct) by the interaction with POBN [68]. When POBN/ethanol spin-trapping system was added to untreated cell suspension, no POBN-$CH(CH_3)OH$ adduct EPR spectrum was observed (Fig. 1A, trace a). The addition of H_2O_2 to cell suspension resulted in small POBN-$CH(CH_3)OH$ adduct EPR signal (Fig. 1A, trace b), while pronounced POBN-$CH(CH_3)OH$ adduct EPR signal was observed after the addition of Fenton reagent to the cell suspension (Fig. 1A, trace c). When POBN-$CH(CH_3)OH$ adduct EPR spectra were measured after 30 min there was no POBN-$CH(CH_3)OH$ adduct EPR signal from untreated cell suspension (Fig. 1B, trace a). The POBN-$CH(CH_3)OH$ adduct EPR signal from the cell suspension treated with H_2O_2 for 30 min (Fig. 1B, trace b) was enhanced twice or three times as compared to POBN-$CH(CH_3)OH$ adduct EPR signal measured immediately after the addition of H_2O_2 (Fig. 1A, trace b). Similarly, POBN-$CH(CH_3)OH$ adduct EPR signal observed 30 min after the addition of Fenton reagent to cell suspension increased ten times (Fig. 1B, trace c) as compared to POBN-$CH(CH_3)OH$ adduct EPR signal measured immediately after the addition of Fenton reagent (Fig. 1A, trace c). To confirm the identification of POBN-$CH(CH_3)OH$ adduct EPR signal, simulation of experimental data was performed (Fig. 1A and B, trace c, dotted line).
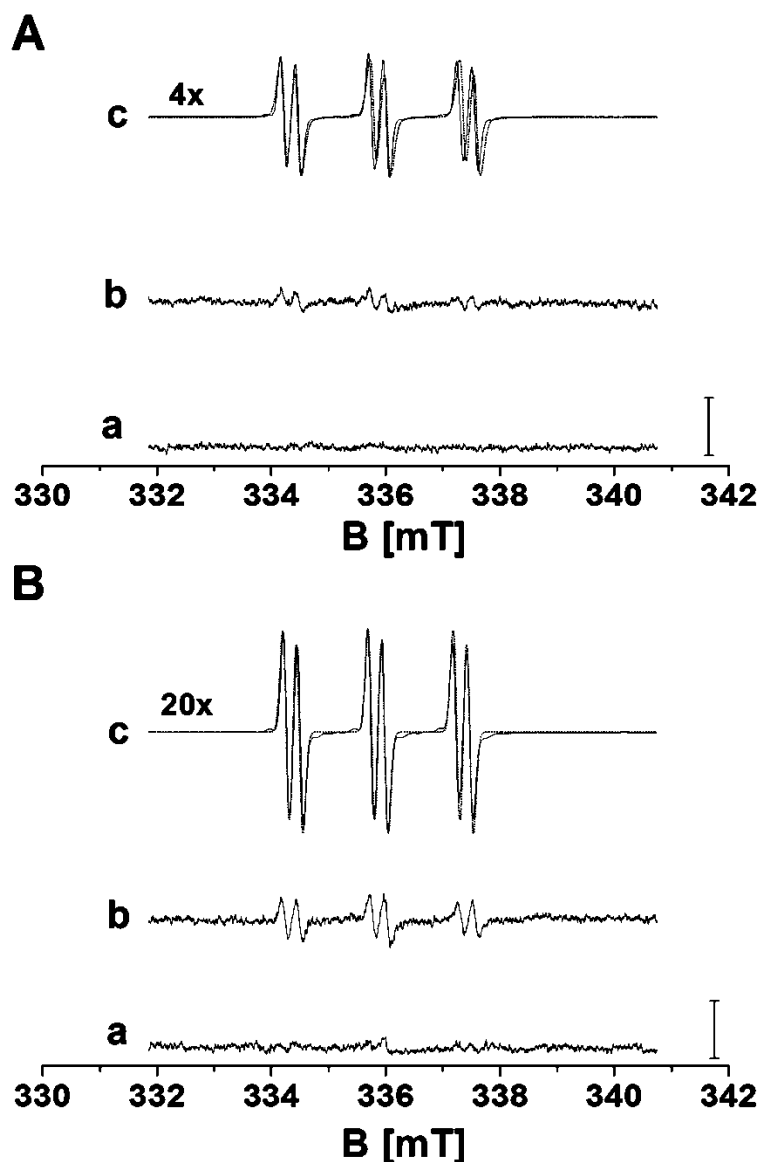
Figure 1: Detection of hydroxyl radical by EPR spin-trapping spectroscopy.

EPR spectra of POBN-CH(CH$_3$)OH adduct were detected 0 min (A) and 30 min (B) after the addition of H$_2$O$_2$ and Fenton reagent to the cell suspension containing U937 cells. EPR POBN-CH(CH$_3$)OH adduct spectra were measured in the control (trace a), H$_2$O$_2$-treated (trace b) and Fenton reagent-treated (trace c) cell suspension in the presence of 100 mM POBN/170 mM ethanol system. Cell suspension was treated with 5 mM H$_2$O$_2$ (b) and Fenton reagent (5 mM H$_2$O$_2$ and 1 mM FeSO$_4$) (c) for 0 min (A) and 30 min (B). In A and B, trace c (dotted line) shows the simulation of POBN-CH(CH$_3$)OH EPR adduct signal using hyperfine coupling constants a^N = 15,75 G, a^H = 2,40 G. Experimental EPR conditions were as follows: microwave power, 10 mW; modulation amplitude, 1 G; modulation frequency, 100 kHz; sweep width, 100 G; scan rate, 1.62 G s^{-1}, gain 500. In B (trace c), to avoid overscaling of POBN-CH(CH$_3$)OH adduct EPR signal, 50 mM POBN/170 mM ethanol system and gain 100 was used. Bars represent 2000 relative units. (Paper III).

The best simulation of experimental data was accomplished using hyperfine coupling constants a^N = 15.75 G, a^H = 2.40 G known to be attributed to POBN-CH(CH₃)OH adduct [68]. These observations reveal that HO$^\bullet$ is formed after the addition of H_2O_2 or Fenton reagent to cell suspension with more pronounced effect observed after the addition of Fenton reagent.

Oxidation of biomolecules

Analysis of lipid peroxidation by MDA HPLC assay

Malondialdehyde, a by-product of lipid peroxidation, was detected in order to monitor oxidative damage of lipids caused by the addition of H_2O_2 and Fenton reagent to cell suspension containing U937 cells. An adaptation of a very rapid and simple isocratic reversed-phase HPLC separation of DNPH-MDA complex with absorption at 310 nm was used to examine the level of lipid peroxidation [67]. Figure 2A shows the chromatogram of DNPH-MDA complex measured in the control (trace a), H_2O_2-treated (trace b) and Fenton reagent-treated (trace c) cell suspension. To estimate the retention time of DNPH-MDA complex, the chromatogram of DNPH-MDA standard was measured (Fig. 2B). The HPLC analysis of MDA-DNPH complex showed that the addition of H_2O_2 to cell suspension caused no enhancement in peak area as compared to untreated cell suspension. The peak area for the Fenton reagent-treated cell suspension was found three times higher compared to the peak area for the control and H_2O_2-treated cell suspension. To quantify the concentration of MDA, standard calibration curve was obtained by plotting the peak area at 310 nm for various MDA concentrations (Fig. 2B, insert). The level of MDA in the control U937 cells and H_2O_2-treated U937 cells was 0.029±0.003 and 0.030±0.003 nmol ml^{-1}, respectively, while in Fenton reagent-treated U937 cells the level of MDA is 0.090±0.020 nmol ml^{-1}. These observations reveal no difference the level of MDA in U937 cells from untreated cell

suspension and cell suspension treated with H_2O_2 while there is significantly increased concentration of MDA in the U937 cells from cell suspension treated with Fenton reagent.
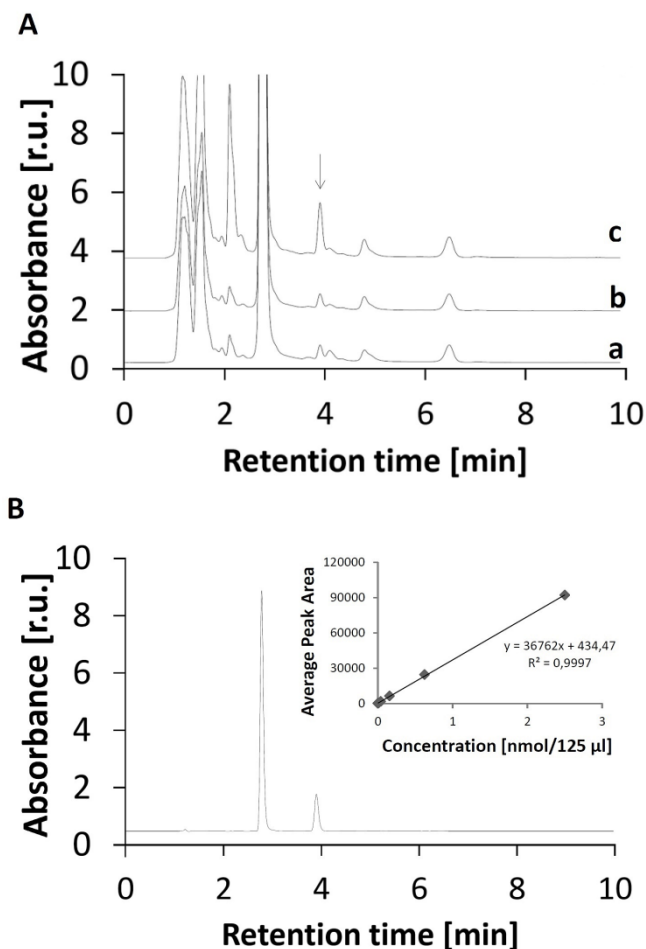

Figure 2: Detection of lipid peroxidation product malondialdehyde by HPLC analysis.
The chromatogram of DNPH-MDA complex in U937 cells (A) and DNPH-MDA standard (B). In A, chromatogram of DNPH-MDA complex was measured in the control (trace a), the H_2O_2-treated (trace b) and the Fenton reagent-treated (trace c) cell suspension containing U937 cells. The cell suspension was treated with 5 mM H_2O_2 (b) and Fenton reagent (5 mM H_2O_2 and 1 mM $FeSO_4$) (c) for 30 min. After the treatment, lipids were isolated and mixed with DNPH. In B, the chromatogram of DNPH-MDA standard shows the retention time of 3 min 50 s. The insert shows the dependence of average peak area on the concentration of DNPH-MDA standard. Based on the calibration curve, the concentrations of DNPH-MDA complex determined from calibration curve were as following: 0.029 ± 0.003 nmol ml^{-1} (control), 0.030 ± 0.003 (H_2O_2) and 0.090 ± 0.020 nmol ml^{-1} (Fenton reagent). The coefficient of determination R^2 was determined as 0.9997. Data are presented as mean values and standard deviations. The mean value represents the average value from at least three measurements. (Paper III).

Analysis of protein carbonylation by dot blot immunoassay

To monitor the oxidative damage of proteins caused by the addition of H_2O_2 and Fenton reagent to the cell suspension containing U937 cells, the protein carbonyl levels were detected using DNPH dot blot immunoassay. The identification of protein carbonyls was facilitated by the derivatization of the carbonyl group with DNPH forming DNP product and by the binding of specific anti-DNP antibodies allowing their detection by imunoblotting analysis. Figure 3 demonstrates dot blot membrane obtained from U937 cells in untreated (A), H_2O_2-treated (B) and Fenton reagent-treated (C) cell suspension. The addition of H_2O_2 to cell suspension 30 min prior to the analysis attenuated protein carbonyl level in U937 cells (Fig. 3B) as compared to control (Fig. 3A). The most significant increase in protein carbonyl level was observed in the U937 cells from Fenton reagent-treated cell suspension (Fig. 3C). The quantification of dot blot membrane performed using densitometry shows that the enhancement in protein carbonyl level observed in U937 cells from H_2O_2-treated and Fenton reagent-treated cell suspension is twice and three times as compared to control, respectively.
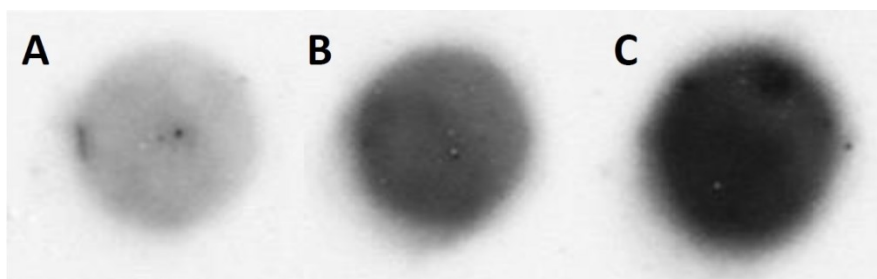

Figure 3: Detection of protein carbonyl compounds by dot blot immunoassay.
Dot blot membrane in the control (A), the H_2O_2-treated (B) and the Fenton reagent-treated (C) cell suspension containing U937 cells. The cell suspension was treated with 5 mM H_2O_2 (B) and Fenton reagent (5 mM H_2O_2 and 1 mM $FeSO_4$) (C) for 30 min. After the treatment, the supernatant containing proteins were pipetted on the membrane and incubated with primary antibody (anti-dinitrophenyl-KLH, rabbit igG fraction, biotinilated) overnight. Furthermore the membrane was incubated with streptavidin-HRP conjugate for 1 h, developed with ECL and chemiluminescence signal was detected on X-ray film. The densitometry results are 0.5±0.2 (control), 1.4±0.2 (H_2O_2-treated), and 2.3±0.3 (Fenton reagent). Data are presented as mean values and standard deviations. The mean value represents the average value from at least three measurements. (Paper III).

These observations indicate that the addition of H_2O_2 and Fenton reagent to cell suspension containing U937 cells resulted in the oxidative damage of proteins with more pronounced effect observed after the addition of Fenton reagent.

Analysis of DNA fragmentation by comet assay

In order to examine the oxidative damage of DNA caused by the addition of H_2O_2 and Fenton reagent to cell suspension containing U937 cells, the DNA fragmentation was measured by comet assay (single cell electrophoresis). The visualization of DNA from tail and head stained by SYBR Green was performed by fluorescence microscopy. Figure 4 shows the comet assay images of U937 cells from untreated (A), H_2O_2-treated (B) and Fenton reagent-treated (C) cell suspension. In the U937 cells from untreated cell suspension, intact comet heads were observed, whereas heads and tails were distinguished in U937 cells from H_2O_2-treated and Fenton reagent-treated cell suspension. Table 1 summarizes the parameters of comet, head and tail determined by the image analysis in the U937 cells from untreated, H_2O_2-treated and Fenton reagent-treated cell suspension. Statistical analysis revealed that most of the parameters are significantly different in U937 cells from H_2O_2-treated and Fenton reagent-treated U937 cell suspension compared to U937 cells from untreated cell suspension, whereas no significant differences were observed between U937 cells from H_2O_2-treated and Fenton reagent-treated cell suspension. These observations indicate that the addition of both H_2O_2 and Fenton reagent to cell suspension caused the fragmentation of DNA in U937 cells with non-significantly higher effect observed after the addition of Fenton reagent.
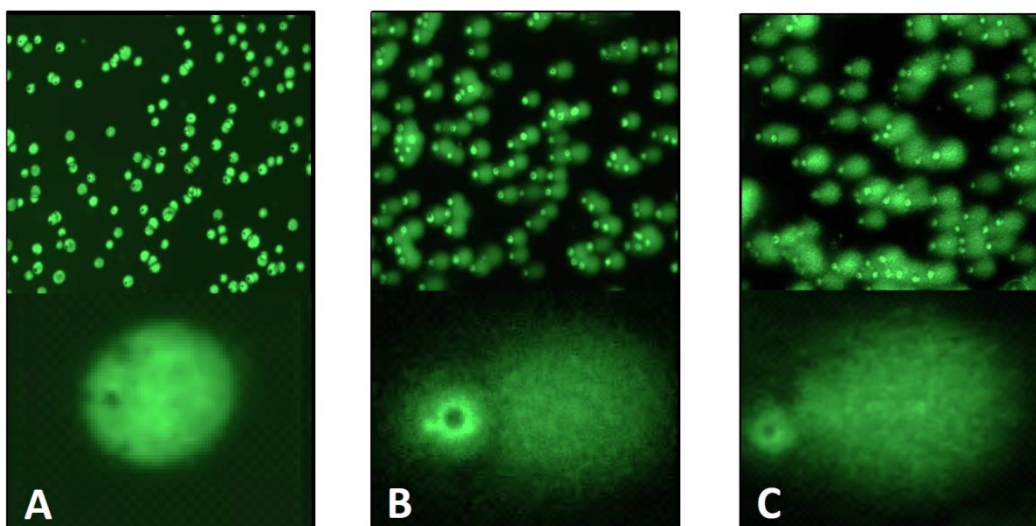
Figure 4: Analysis of DNA strand breaks by Comet assay

Comet assay of the control (A), the H_2O_2-treated (B) and the Fenton reagent-treated (C) U937 cells. The U937 cells were treated with 5 mM H_2O_2 (B) and Fenton reagent (5 mM H_2O_2 and 1 mM $FeSO_4$) (C) for 30 min. After the treatment, U937 cells were stained by SYBR Green. (Paper III).

Table 1: Analysis of the medians of comet, head, and tail parameters in the control, the H_2O_2-treated and the Fenton reagent-treated U937 cells. Data are presented as mean values and standard deviations. The mean value represents the average value from at least three measurements. (Paper III).

	Length [μm]	Height [μm]	Area [μm²]	Intensity [r.u.]	Mean Intensity [r.u.]
Comet					
Control	20 ± 2	18 ± 2	301 ± 71	71506 ± 18571	51 ± 5
H₂O₂	44 ± 2	24 ± 2	762 ± 66	99182 ± 7767	27 ± 1
Fenton	51 ± 6	25 ± 3	301 ± 71	123451 ± 18571	51 ± 5
Head	Diameter [μm]	%DNA	Area [μm²]	Intensity [r.u.]	Mean Intensity [r.u.]
Control	18 ± 2	91 ± 4	262 ± 48	65320 ± 16978	52 ± 7
H₂O₂	13 ± 1	30 ± 2	178 ± 15	27219 ± 1385	31 ± 5
Fenton	10 ± 1	21 ± 10	141 ± 32	24705 ± 7742	31 ± 2
Tail	Length [μm]	%DNA	Area [μm²]	Intensity [r.u.]	Mean Intensity [r.u.]
Control	2 ± 1	8 ± 4	31 ± 21	5888 ± 3993	42 ± 9
H₂O₂	30 ± 3	69 ± 3	524 ± 36	64238 ± 9192	26 ± 1
Fenton	39 ± 8	78 ± 10	659 ± 161	94581 ± 32988	29 ± 2

Formation of triplet excited carbonyls detected by ultra-weak photon emission

To study the kinetics of ultra-weak photon emission decay, one-dimensional ultra-weak photon emission was measured using PMT. Spontaneous ultra-weak photon emission from cell suspension containing U266 cells measured in the absence of H_2O_2 showed steady-state level, whereas the addition of H_2O_2 at the time of 30 min induced pronounced enhancement of photon emission followed by slow decay in photon emission (Fig. 5A). To confirm that ultra-weak photon emission is in the blue-green region of the spectrum assigned to $^3(R=O)^*$, the ultra-weak photon emission was measured in the presence of long-pass edge filter (600 nm). Figure 5B shows that ultra-weak photon emission was significantly suppressed in the presence of the long-pass edge filter. To determine the participation of $^1O_2$ in ultra-weak photon emission originated from red region of the spectrum, the effect of histidine on ultra-weak photon emission was measured. Figure 5C demonstrates that the ultra-weak photon emission in the red region was almost fully suppressed in the presence of histidine. These results prove that most of the ultra-weak photon emission originates from the blue-green region of the spectrum known to be associated with the photon emission of $^3(R=O)^*$. Moreover, the measurement of one-dimensional ultra-weak photon emission reveales that the formation of $^3(R=O)^*$ starts immediately after the addition of H_2O_2 to the cell suspension and decay slowly.
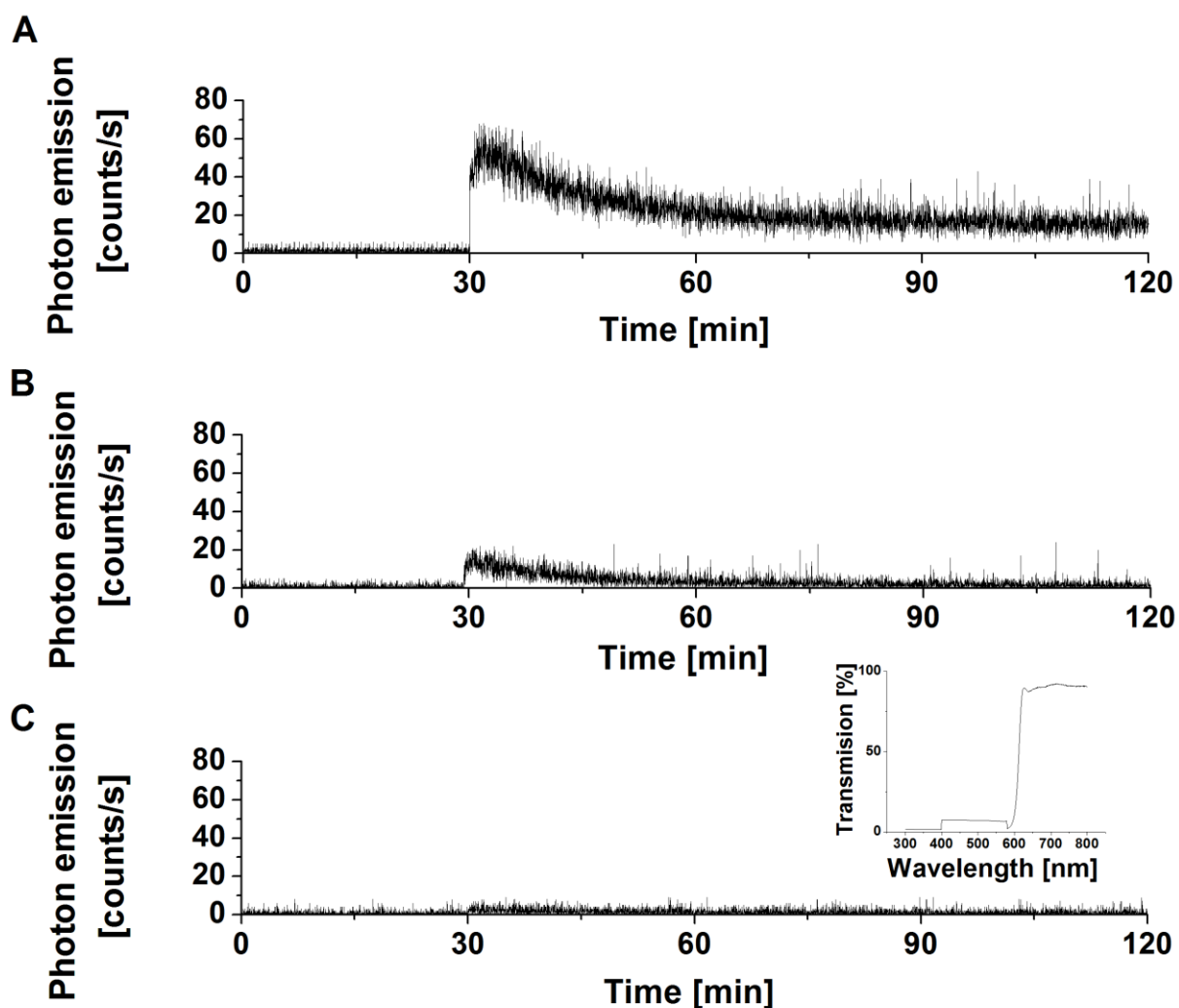
Figure 5: Triplet excited carbonyl detection by one-dimensional ultra-weak photon emission
One-dimensional ultra-weak photon emission from cell suspension was measured by low-noise PMT. After 10 min of dark period, spontaneous ultra-weak photon emission was measured for 30 min. Consequently, 5 mM H_2O_2 was added to the cell suspension. In B, the ultra-weak photon emission from cell suspension treated by the addition of 5 mM H_2O_2 was measured in the presence of the long-pass edge filter (600 nm). Insert shows transmission spectrum of long-pass edge filter. In C, the effect of 10 mM histidine on ultra-weak photon emission from cell suspension is shown. (Paper IV).

To visualize the formation of $^3(R=O)^*$ in the cell suspension containing U266 cells treated with H_2O_2, the two-dimensional ultra-weak photon emission was detected using a highly sensitive CCD camera. Figure 6 shows two-dimensional images of the ultra-weak photon emission measured from cell suspension after the addition of H_2O_2. The treatment of cell suspension with H_2O_2 resulted in the pronounced increase in ultra-weak photon emission

compared to control. To quantify the differences in ultra-weak photon emission from cell suspension treated with H_2O_2, the spatial profile of photon emission in the middle strip of the image was used. The number of counts of ultra-weak photon emission from cell suspension measured in the absence of H_2O_2 was under the detection limit of CCD camera. These results indicate that the addition of H_2O_2 to cell suspension containing U266 cells causes the formation of $^3(R{=}O)^*$.
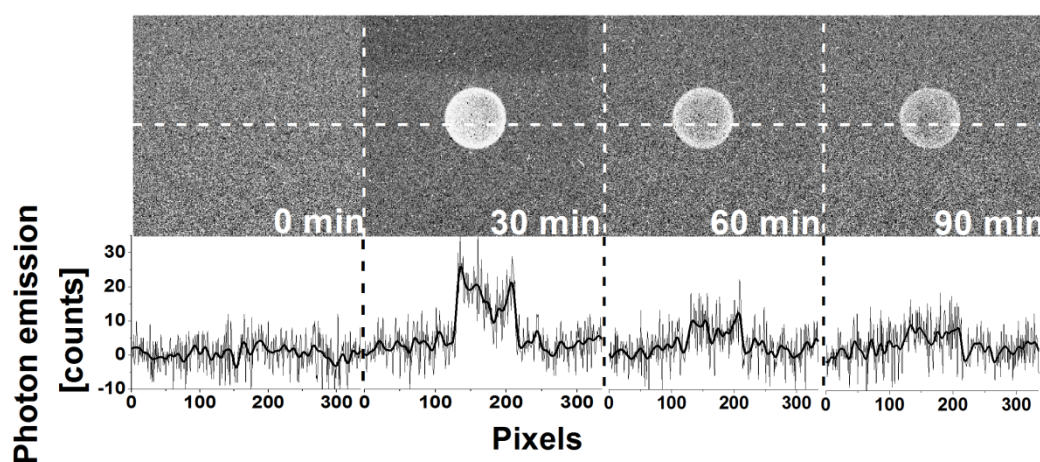

**Figure 6: Triplet excited carbonyl by two-dimensional imaging of ultra-weak photon emission**
Two-dimensional imaging of the ultra-weak photon emission was measured from the cell suspension by a highly sensitive CCD camera. Prior to the measurements, the cell suspension was kept in the dark for 10 min. After dark period, ultra-weak photon emission was measured from untreated cell suspension. Consequently, a set of three images of ultra-weak photon emission was measured after the addition of H_2O_2 to cell suspension for time period indicated in figure. The images of ultra-weak photon emission were measured with the integration time of 30 min. The bottom panel shows the spatial profile of photon emission in the middle strip of the image. Y axis denotes the number of counts accumulated after 30 min, whereas X axis denotes the pixel of the image. (Paper IV).

Formation of singlet oxygen

Formation of singlet oxygen detected by EPR spin-trapping spectroscopy

To study whether oxidative damage of biomolecules generates $^1O_2$, EPR spin-trapping technique was used to monitor the formation of $^1O_2$ in H_2O_2-treated and Fenton reagent-treated cell suspension containing U937 cells. The spin-trapping was accomplished by utilizing the oxidation of hydrophilic diamagnetic TMPD by $^1O_2$ know to yield paramagnetic

2, 2, 6, 6-tetramethyl-4-piperidone-1-oxyl (TEMPONE). The addition of TMPD to untreated cell suspension resulted in low TEMPONE EPR signal (Fig. 7A-B). When TEMPONE EPR spectra were measured after the addition of H_2O_2 to the cell suspension, TEMPONE EPR signal was observed (Fig. 7C). Figure 7D shows that TEMPONE EPR signal increased within 10 min followed by gradual decrease. The gradual decrease of TEMPONE EPR signal was likely caused by the oxidation of TEMPONE resulting in the formation of EPR silent oxidized TEMPONE. These observations indicate that $^1O_2$ is formed after the addition of H_2O_2 and Fenton reagent to the cell suspension. When TEMPONE EPR spectra were measured after the addition of Fenton reagent, significant TEMPONE EPR signal was observed (Fig. 7E). Figure 7F shows that TEMPONE EPR signal increased within 10 min followed by steady-state level. Comparison of TEMPONE EPR signals showed TEMPONE EPR signals measured after the addition of Fenton reagent is double compared to TEMPONE EPR signals measured after the addition of H_2O_2. Figure 7B (trace c, dotted line) shows the simulation of TEMPONE EPR signal using hyperfine coupling constants $a^N = 16$ G, known to be attributed to TEMPONE [70]. These findings prove the formation of $^1O_2$ after the addition of H_2O_2 or Fenton reagent to cell suspension containing U937 cells with more pronounced effect observed after the addition of Fenton reagent.
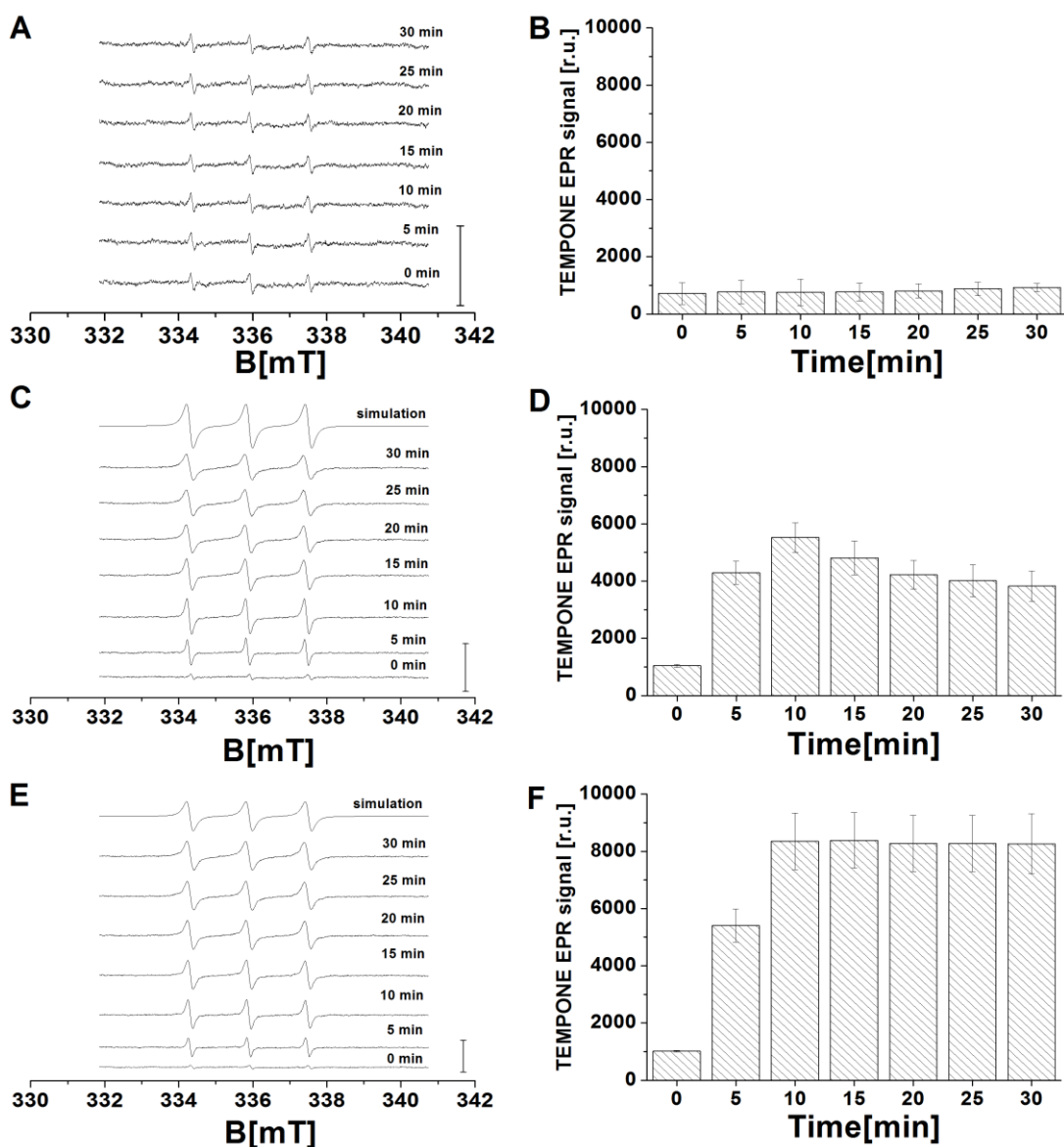
Figure 7: Detection of singlet oxygen by EPR spin-trapping spectroscopy.

TEMPONE EPR spectra were measured in the control (A and B), the H_2O_2-treated (C and D) and the Fenton reagent-treated (E and F) cell suspension containing U937 cells in the presence of 100 mM TEMPD. Cell suspension was treated with no addition (A), 5 mM H_2O_2 (C) and Fenton reagent (5 mM H_2O_2 and 1 mM $FeSO_4$) (E) for a period indicated in figure. In C and E, top traces show the simulation of TEMPONE EPR signal using hyperfine coupling constants a^N = 16 G. Bar graphs represent the hight of the middle peak of TEMPONE EPR signal in the control (B), the H_2O_2-treated (D) and the Fenton reagent-treated (F) U937 cells. Experimental EPR conditions were as follows: microwave power, 10 mW; modulation amplitude, 1 G; modulation frequency, 100 kHz; sweep width, 100 G; scan rate, 1.62 G s-1, gain 500. Bars represent 4000 (A) and 8000 (C and E) relative units. Data are presented as mean values and standard deviations. The mean value represent the average value from at least three measurements. (Paper III).

To study the kinetics of the $^1O_2$ formation during longer time period after the addition of H_2O_2 to cell suspension containing U266 cells, EPR spin-trapping technique was used. The time periods of 0-30, 30-60, and 60-90 min was studied. Figure 8 shows the formation of TEMPONE EPR adduct during the time perion indicated in figure after the addition of H_2O_2 to the cell suspension. To confirm that EPR signal is attributed to TEMPONE the EPR spectrum of pure TEMPONE was used. The simulation of TEMPONE EPR spectra using one spectral component with the hyperfine coupling constant $a^N = 16$ G provided agreement with the hyperfine coupling constant described for TEMPONE. These results indicate that the formation of $^1O_2$ in the cell suspension occurs predominantly during the 0-30 min time period.
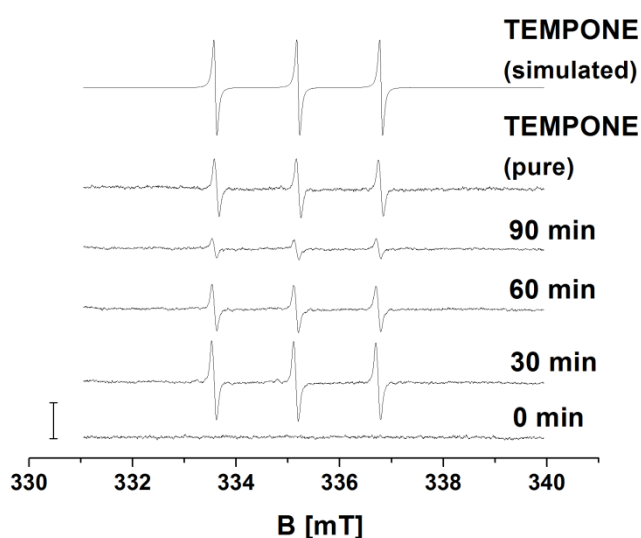
Figure 8: Detection of singlet oxygen by EPR spin-trapping spectroscopy
TEMPONE EPR spectra were detected from cell suspension containing U266 cells treated with 5 mM H_2O_2 for the period indicated in figure. 50 mM TEMPD was added to cell suspension 30 min prior to the measurement. Pure TEMPONE EPR signal was detected using 20 nM TEMPONE. The simulation of TEMPONE EPR spectra was done using hyperfine splitting constant $a^N = 16$ G. Bar represents 3000 relative units. (Paper IV).

Formation of singlet oxygen detected by laser scanning microscopy

To visualize the formation of $^1O_2$ in U937 cells after the addition of H_2O_2 and Fenton reagent to the cell suspension containing U937 cells, the SOSG fluorescence was measured by the confocal laser scanning microscopy (Fig. 9A). In order to quantify the $^1O_2$ formation, the intensity of SOSG fluorescence was evaluated (Fig. 9B). Negligible SOSG fluorescence was recorded in the U937 cells from untreated cell suspension. In order to confirm that the SOSG fluorescence origins from the interaction of SOSG with $^1O_2$, the effect of histidine on the SOSG fluorescence was measured. No difference in SOSG fluorescence was found in the U937 cells from cell suspension incubated with histidine. The addition of H_2O_2 to the cell suspension resulted in a pronounced SOSG fluorescence. The effect of H_2O_2 addition was significantly decreased in the presence of histidine. The addition of Fenton reagent to the cell suspension caused SOSG fluorescence comparable to that in the H_2O_2-treated cell suspension. These results indicate that addition of H_2O_2 and Fenton reagent to the cell suspension containing U937 cells results in the formation of $^1O_2$ in U937 cells.
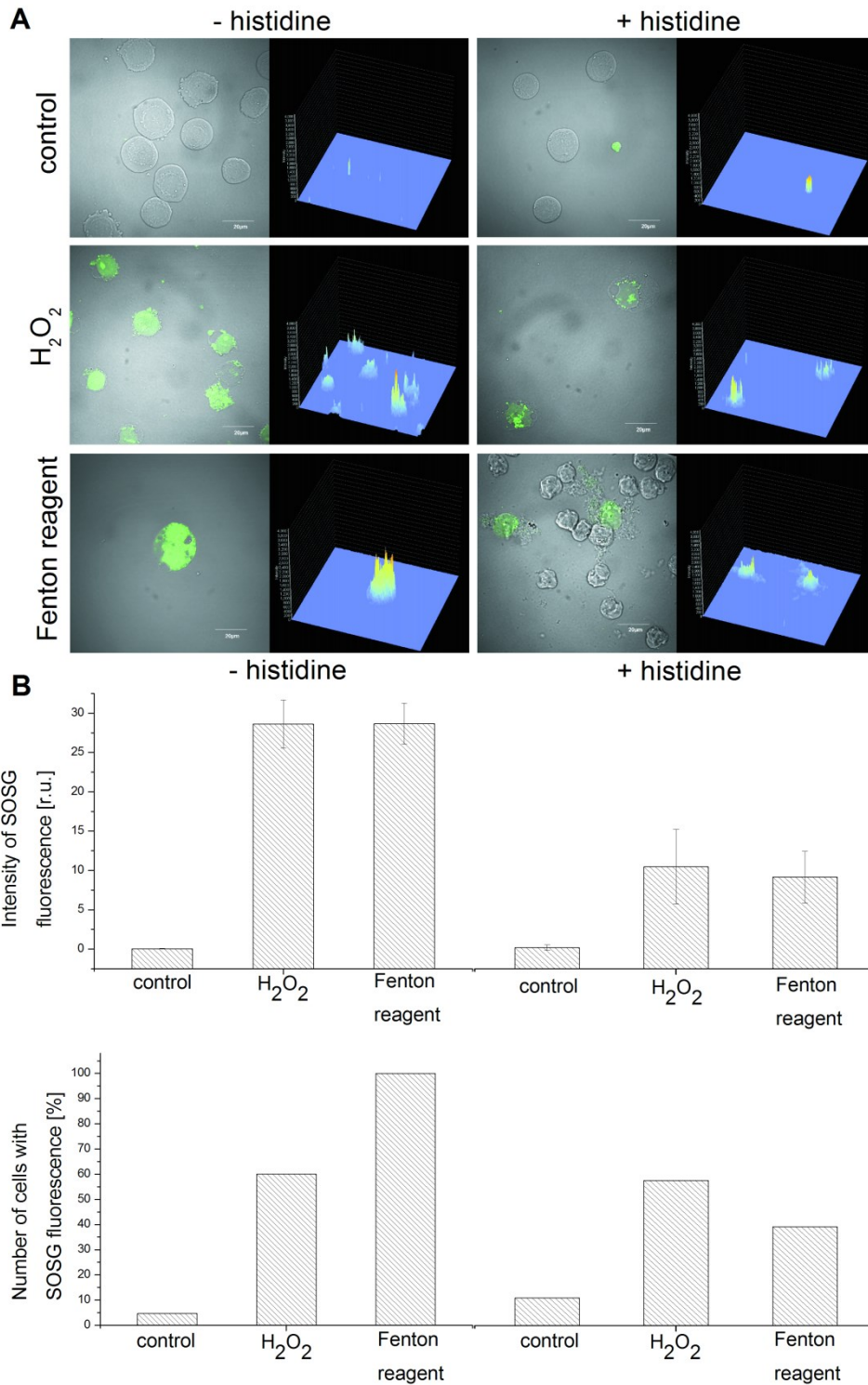
Figure 9: Singlet oxygen imaging by confocal laser scanning microscopy

The SOSG fluorescence from U937 cells was measured after the addition of 5 mM H_2O_2 and Fenton reagent (5 mM H_2O_2 and 1 mM $FeSO_4$) by confocal laser scanning microscopy. 50 µM SOSG was added 30 min prior to the data collection to the U937 cells. In A, left column shows the combination of Nomarski DIC and SOSG fluoresencence (λ_{em} = 505-525 nm) channels and right column the integral distribution of SOSG fluorescence. In B, the intensity of SOSG fluorescence (upper graph) and the percentage of cells showing the SOSG fluorescence (lower graph) are shown. Data are presented as mean values and standard deviations. The mean value represents the average value from five to ten representative microphotographs per variant. (Paper III).

To visualize the kinetic of the $^1O_2$ formation in U266 cells caused by the addition of H_2O_2 to the cell suspension containing U266 cells, SOSG fluorescence was detected by confocal laser scanning microscopy. Figure 10A shows the formation of $^1O_2$ in the U266 cells from cell suspension treated with H_2O_2 in the time period of 0-30, 30-60, 60-90 min after the addition of H_2O_2. Negligible SOSG fluorescence was detected in the U266 cells from untreated cell suspension. SOSG fluorescence was pronouncedly stronger in the U266 cells from H_2O_2-treated cell suspension compared to control. Figure 10B represents the integral distribution of SOSG fluorescence intensity within the corresponding upper image. Although the SOSG was originally devised for extracellular applications, several studies reported its limited penetration inside of cells [71, 72]. To test whether SOSG penetrates into the U266 cells, SOSG fluorescence was measured in the multiple layers of samples (Fig. 11). The presence of SOSG fluorescence in the multiple layers of cells reveales the formation of $^1O_2$ whithin U266 cells following the addition of H_2O_2 to the cell suspension containing U266 cells.
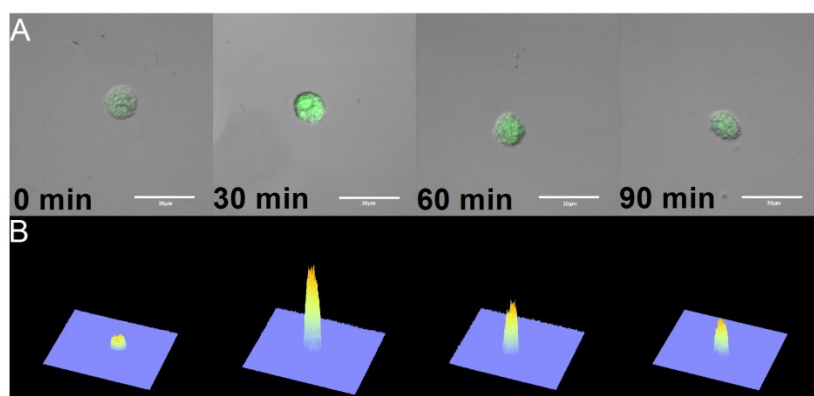
Figure 10: Singlet oxygen imaging by confocal laser scanning microscopy

The green fluorescence of SOSG within U266 cells treated with 5 mM H_2O_2 for the time period indicated in figure was examined by a confocal laser scanning microscope. 50 μM SOSG was added to U266 cells 30 min prior to the data collection. In A, the individual representative cells of each time variant are shown in the images combining Nomarski DIC and SOSG fluorescence (λ_{em} = 505-525 nm) channels. In B, the integral distribution of the SOSG fluorescence intensity is shown within the corresponding upper images. The bar represents 30 μm. (Paper III).
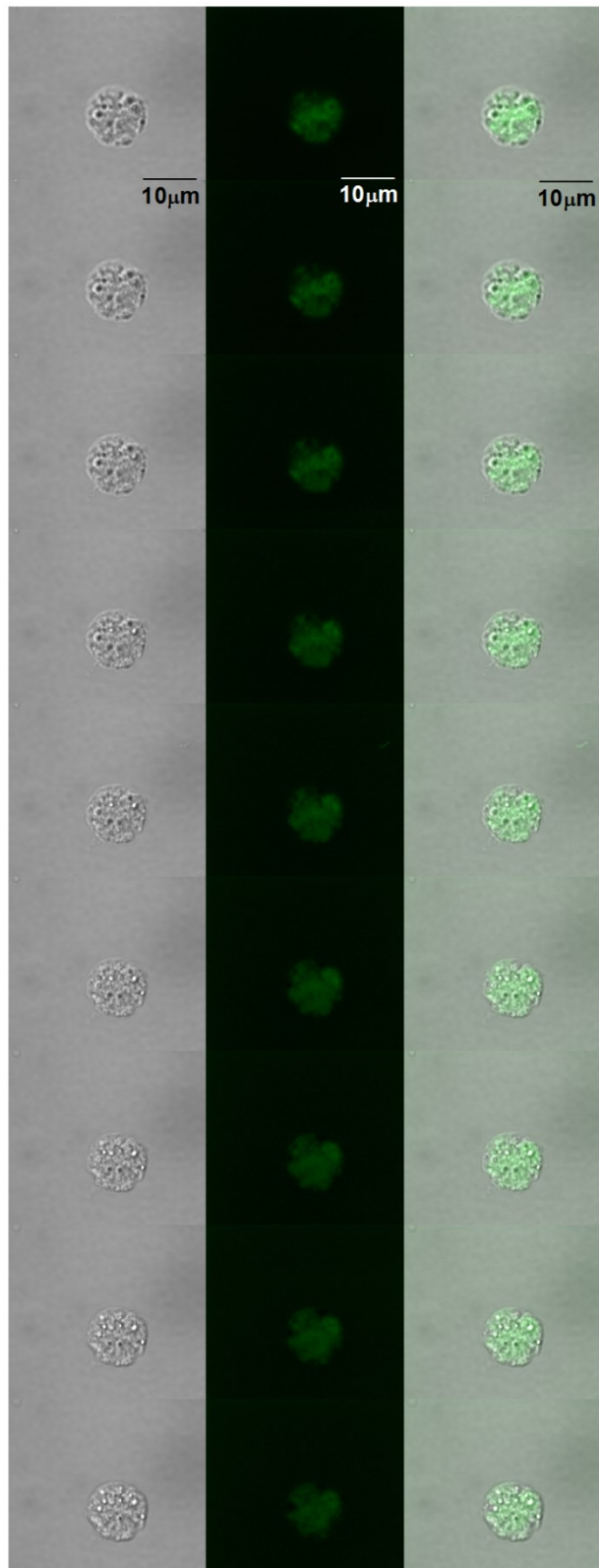
**Figure 11: Singlet oxygen imaging in the multiple layers of the sample**

The step in between different pictures is 0.5 μm. Three channels are presented: Nomarsky DIC (left column), SOSG fluorescence (λ_{em}=505-525 nm) (middle column) and the combination of Nomarski DIC and SOSG fluorescence (right column). U266 cells were treated with 5 mM H_2O_2 for 30 min. Other parameters are same as in Fig. 10. (Paper IV).

Discussion

In this thesis, the oxidation of biomolecules such as lipids, proteins and nuclei acids by $HO^\bullet$ was studied after the addition of H_2O_2 and Fenton reagent to the cell suspension. The experimental data provided show that hydrogen abstraction by $HO^\bullet$ initiates a cascade of oxidative reactions leading to lipid peroxidation, protein carbonylation and DNA fragmentation. The oxidation of biomolecules by ROS is accompanied by the formation of electronically excited species. In this thesis, the formation of $^3(R=O)^*$ and $^1O_2$ after the addition of H_2O_2 and Fenton reagent to cell suspension was studied. Comparison of the results revealed similar kinetics of formation of both electronically excited species. The main goal of this thesis was to confirm the formation of electronically excited species in the cell suspension upon the exposure to oxidative conditions and to suggest possible mechanisms of their formation.

Formation of hydroxyl radical

EPR spin-trapping data showed that the addition of H_2O_2 and Fenton reagent to cell suspension containing U937 cells caused the formation of $HO^\bullet$ via Fenton reaction. In this reaction, a reduced metal ion reacts with H_2O_2 forming an oxidized metal ion and $HO^\bullet$ [12]. Several types of endogenous metal ions such as iron, copper, manganese, zinc, chromium, cobalt, nickel and vanadium were shown to reduce H_2O_2 to $HO^\bullet$ [12]. It is well known that endogenous iron ions are coordinated to active enzyme site in metalloproteins or stored in a ubiquitous protein called ferritin [73]. Following the addition of H_2O_2 to cell suspension, $HO^\bullet$ is formed by the reaction of H_2O_2 with either endogenous metal ions in the cells or transition metal ions present in the growth medium. Due to the lower concentration of endogenous metal ions and metal ions present in the medium compared to the concentration of

exogenously added iron, the formation of HO$^\bullet$ after the addition of H_2O_2 is significantly lower compared to the addition of Fenton reagent. As the high reactivity of HO$^\bullet$ restricts diffusion of HO$^\bullet$ from the site of its formation, HO$^\bullet$ formed by the reaction of H_2O_2 with endogenous metal ions oxidizes biomolecules solely in the close proximity to the site of its formation [12].

Oxidative damage initiated by hydroxyl radical

Lipid peroxidation

The HPLC analysis of MDA-DNPH complex showed that the addition of H_2O_2 to cell suspension containing U937 cells has no effect on lipids, whereas the addition of Fenton reagent to the cell suspension caused pronounced lipid peroxidation. The observation that no MDA-DNPH complex formation was observed after the addition of H_2O_2 to the cell suspension suggests that H_2O_2 has no capability to directly initiate lipid peroxidation [74] due to the fact than no metal ions are bound to lipids [2]. The observation that lipid peroxidation was detected after the addition of Fenton reagent to cell suspension indicates that the presence of exogenous iron ions allows the formation of HO$^\bullet$ with no site-specificity and thus HO$^\bullet$ formed in the close proximity of membranes initiates lipid peroxidation. Abstraction of hydrogen atom from lipid by the HO$^\bullet$ results in the formation of lipid R$^\bullet$ (Scheme I, reaction 6). In the propagation step, lipid R$^\bullet$ reacts with molecular oxygen forming ROO$^\bullet$ (Scheme I, reaction 7) known to react with another lipid molecule resulting in the formation of another lipid R$^\bullet$. In the termination step, lipid peroxidation is terminated by either cyclization of ROO$^\bullet$ to cyclic endoperoxide or ROOR or by the recombination of two ROO$^\bullet$ producing ROOOOR (Scheme I, reaction 12) decomposing to $^1O_2$ via Russell mechanism [75] (Scheme I, reaction 23). Cyclic endoperoxide is known to decompose to MDA, while the decomposition of ROOR results in the formation of $^3(R{=}O)^*$ (Scheme I, reaction 14).

Protein carbonylation

The addition of H_2O_2 and Fenton reagent to cell suspension containing U937 cells resulted in the oxidative damage of proteins with significantly higher effect observed after the addition of Fenton reagent. These results correlate with the EPR spin-trapping data which showed significantly higher formation of $HO^\bullet$ in the cell suspension treated with Fenton reagent. It is well known that protein carbonylation occurs both on the protein side chain and the protein backbone. On the protein side chain, the carbonylation of protein proceeds via direct oxidation or chain reaction. The direct oxidation of protein side chains (especially of Pro, Arg, Lys, and Thr) results in the formation of carbonyl groups [76]. In the chain reaction, the hydrogen abstraction from an amino acid residue by $HO^\bullet$ results in the formation of protein $R^\bullet$ (Scheme I, reaction 6). Protein $R^\bullet$ can subsequently react with molecular oxygen forming protein $ROO^\bullet$ (Scheme I, reaction 7). The cyclization of protein $ROO^\bullet$ can result in the formation of ROOR which subsequently decomposes to $^3(R=O)^*$. The recombination of two protein $ROO^\bullet$ gives a raise to unstable ROOOOR (Scheme I, reaction 12). Subsequent decomposition of ROOOOR can result in the formation of $^1O_2$ via Russell mechanism (Scheme I, reaction 23) or the formation of two $RO^\bullet$ (Scheme I, reaction 9). Once $RO^\bullet$ is formed, it can undergo through rearrangement of electron resulting in the formation of carbonyl radical and carbonyl compound on the protein side chain. On the protein backbone, the formation of $RO^\bullet$ can also result in the oxidative cleavage of protein backbone by either the α-amidation pathway or by oxidation of glutamyl side chains leading to the formation of carbonyl groups [21, 77]. The oxidation of proteins prior to the lipids after the addition of H_2O_2 to the cell suspension is in a good agreement with the previously reported findings that the proteins are the initial target in the cells after the exposure to radicals [78-82].

DNA fragmentation

The addition of both H_2O_2 and Fenton reagent to U937 cells caused the fragmentation of DNA with non-significantly higher effect observed after the addition of Fenton reagent. It was previously reported that no DNA strand breaks were formed during the interaction of H_2O_2 and isolated DNA [83], whereas $HO^\bullet$ formed via Fenton reaction forms DNA strand breaks [84, 85]. At least five main classes of oxidative damage caused by $HO^\bullet$ have been proposed including oxidized bases, abasic sites, DNA-DNA intra-strand adducts, DNA strand breaks and DNA-protein cross-links. It has been proposed that the extent of DNA strand breaking by $HO^\bullet$ is governed by the accessible surface areas of the hydrogen atoms of the DNA backbone [86].

Triplet excited carbonyls formation

Two-dimensional ultra-weak photon emission confirms the formation of $^3(R=O)^*$ upon the addition of H_2O_2 to cell suspension containing U266 cells. Based on the results obtained by one-dimensional ultra-weak photon emission, it is concluded here that the formation of $^3(R=O)^*$ occurs immediately after the addition of H_2O_2 to the cell suspension. Data presented in this study are in an agreement with previously published work. Spectral analysis of the ultra-weak photon emission from different samples such as rat perfused lung, rat brain and liver homogenate, spinach mitochondria, cotyledons of etiolated seedlings of *Cicer arietinum* L., DNA, hemodialysis plasma cells, esophageal carcinoma cell line, porcine ex-vivo skin model induced by different treatment, showed that ultra-weak photon emission originates mostly from $^3(R=O)^*$ [51, 52, 56, 57, 61, 87, 88]. Several lines of evidence have been provided that $^3(R=O)^*$ is formed by decomposition of ROOR or ROOOOR [29, 42, 43].

Triplet excited carbonyls by 1,2-dioxetane decomposition

1,2-dioxetane is formed either by the cycloaddition of $^1O_2$ to the lipid and proteins (Scheme I, reaction 10) or by the cyclisation of $ROO^\bullet$ (Scheme I, reaction 11). The decomposition of ROOR involves the cleavage of oxygen-oxygen and carbon-carbon bonds by two different mechanisms. The concerted mechanism involves the simultaneous cleavage of oxygen-oxygen and carbon-carbon bonds. The diradical mechanism is a two-step reaction involving the cleavage of oxygen bound prior to the cleavage of carbon-carbon bond [31]. Both reactions result in the formation of $^3(R{=}O)^*$ (Scheme I, reaction 14).

Triplet excited carbonyls by tetroxide decomposition

Tetroxide is formed by the recombination of two $ROO^\bullet$ (Scheme I, reaction 12). It has been demonstrated that t-butyl hydroperoxide does not participate in the ROOOOR formation due to the fact that the presence of α-hydrogen is required in order to undergo the Russell pathway [39, 40]. Based on this observation, it was established that solely the primary and secondary $ROO^\bullet$ are involved in the ROOOOR formation, whereas the tertiary $ROO^\bullet$ undergoes propagation of lipid peroxidation and protein oxidation. While the formation of $^3(R{=}O)^*$ by the decomposition of ROOOOR is theoretically possible (Scheme I, reaction 15), experiments shown that the quantum yield of $^3(R{=}O)^*$ is less than 0.1% in the chemical system and therefore it is suggested here that this reaction occurs only in the growth medium.

Singlet oxygen formation

The formation of $^1O_2$ was detected after the addition of H_2O_2 and Fenton reagent to cell suspension containing U937 cells. These observations indicate that the formation of $^1O_2$ is closely associated with damage of lipids, proteins and DNA. Several lines of evidence have been provided that $^1O_2$ is formed by decomposition of high-energy intermediates such as dioxetane and ROOOOR formed during the oxidative damage of lipids, proteins and DNA.

Based on the data obtained from the cell suspension containing U937 or U266 cells, it is concluded here that the formation of $^1O_2$ occurs predominantly during the first 30 min after the addition of H_2O_2 to the cell suspension. It has been previously demonstrated that SOSG is unable to penetrate into the CNE2 cells [72]. However, it was demonstrated that SOSG can penetrate HeLA cells if cultivated in a special medium lacking proteins [71]. Hereby, it was confirmed that SOSG can penetrate both U937 and U266 cells. The formation of $^1O_2$ within the U937 cells was about the same in the H_2O_2-treated sample and the Fenton reagent-treated U937 cells, while the amount of cells in which $^1O_2$ was produced was double in the Fenton reagent-treated U937 cells compared to the H_2O_2-treated U937 cells. The visualization of the $^1O_2$ formation in the multiple layers of samples confirmed that the $^1O_2$ was produced inside the U266 cells. These results clearly show that U266 cells are oxidized upon the exposure of the cell suspension to H_2O_2 with the outcome of $^1O_2$ formation.

Singlet oxygen by 1,2-dioxetane decomposition

Dioxetane is formed via two different mechanisms comprising the cycloaddition of $^1O_2$ to biomolecules or the cyclization of $ROO^\bullet$ [41] (Scheme I, reaction 10-11). Here, it is proposed that the formation of dioxetane takes place during the physiological and pathological conditions since the concentration of $ROO^\bullet$ is unlikely high enough for the formation of $ROOOOR$ via recombination of $ROO^\bullet$. Unstable dioxetane subsequently undergoes the decomposition to $^3(R=O)^*$ and R=O. The excitation energy from $^3(R=O)^*$ is transferred to molecular oxygen resulting in the formation of $^1O_2$ [29, 89] (Scheme I, reaction 21). It is suggested that the decomposition of dioxetane is responsible for $^1O_2$ formation after the addition of H_2O_2 and Fenton reagent to the cell suspensions.

Singlet oxygen by tetroxide decomposition

It was previously reported that lipid and DNA hydropexides can be decomposed to ROO$^\bullet$ in the presence of metal ions, cytochrome c, peroxynitrite, chloroperoxide, and hypochlorous acid [22, 90, 91]. It has been previously suggested that the recombination of two ROO$^\bullet$ occurs mainly in chemical system or under high oxidative damage conditions. The recombination of two ROO$^\bullet$ forms unstable ROOOOR (Scheme I, reaction 12) which decompose to either $^1O_2$, carbonyl and ROH (Scheme I, reaction 23) or molecular oxygen, $^3(R=O)^*$ and ROH (Scheme I, reaction 16). Furthermore the $^3(R=O)^*$ can react with the molecular oxygen and form $^1O_2$ [29] (Scheme I, reaction 21). It has been established in the chemical system that the formation of $^1O_2$ by the recombination of ROO$^\bullet$ is 3-4 magnitude higher compared to the formation of $^3(R=O)*$ formed the recombination of ROO$^\bullet$ [49]. It is suggested here that the recombination of two ROO$^\bullet$ takes place predominantly in the growth medium rather than inside the cells.

Conclusions

- The addition of both H_2O_2 and Fenton reagent to the cell suspension resulted in the oxidative damage of proteins and DNA, while lipids were oxidized only upon the exposure to Fenton reagent.

- The formation of both electronically excited species in the cell suspension was confirmed.

- The formation of $^3(R{=}O)^*$ in the cell suspension treated with H_2O_2 was confirmed, and the results indicate that $^3(R{=}O)^*$ are the main source of ultra-weak photon emission from cell suspension after the addition of H_2O_2.

- The singlet oxygen formation in the cell suspension treated with both H_2O_2 and Fenton reagent was confirmed by EPR spin-trapping spectroscopy.

- The formation of $^1O_2$ whitin both U937 and U266 cells was confirmed by the confocal laser scanning microscopy.

References

[1]   Pospíšil, P. Production of reactive oxygen species by photosystem II. *Biochimica Et Biophysica Acta-Bioenergetics* **1787:**1151-1160; 2009.

[2]   Halliwell, B.; Gutteridge, J. M. C. *Free radical in biology and medicine.* New York: Oxford University Press; 2007.

[3]   Brieger, K.; Schiavone, S.; Miller, F. J.; Krause, K. H. Reactive oxygen species: from health to disease. *Swiss Medical Weekly* **142**; 2012.

[4]   Singh, P. K.; Shiha, M. J.; Kumar, A. Antibacterial responses of retinal Muller glia: production of antimicrobial peptides, oxidative burst and phagocytosis. *Journal of Neuroinflammation* **11**; 2014.

[5]   Dahlgren, C.; Karlsson, A.; Bylund, J. Measurement of respiratory burst products generated by professional phagocytes. *Methods in Molecular Biology* **412:**349-363; 2007.

[6]   Han, D.; Williams, E.; Cadenas, E. Mitochondrial respiratory chain-dependent generation of superoxide anion and its release into the intermembrane space. *Biochemical Journal* **353:**411-416; 2001.

[7]   Lambert, A. J.; Brand, M. D. Superoxide production by NADH: ubiquinone oxidoreductase (complex I) depends on the pH gradient across the mitochondrial inner membrane. *Biochemical Journal* **382:**511-517; 2004.

[8]   Asada, K. Production and scavenging of reactive oxygen species in chloroplasts and their functions. *Plant Physiology* **141:**391-396; 2006.

[9]   Pospíšil, P. Molecular mechanisms of production and scavenging of reactive oxygen species by photosystem II. *Biochimica et Biophysica Acta-Bioenergetics* **1817:**218-231; 2012.

[10]   Turrens, J. F. Mitochondrial formation of reactive oxygen species. *Journal of Physiology-London* **552:**335-344; 2003.

[11]   Halliwell, B.; Clement, M. V.; Long, L. H. Hydrogen peroxide in the human body. *Febs Letters* **486:**10-13; 2000.

[12]   Goldstein, S.; Meyerstein, D.; Czapski, G. The Fenton reagents. *Free Radical Biology and Medicine* **15:**435-445; 1993.

[13]   Trenam, C. W.; Blake, D. R.; Morris, C. J. Skin Inflammation: Reactive Oxygen Species and the Role of Iron. *Journal of Investigative Dermatology* **99:**675-682; 1992.

[14]   Takeshita, K.; Takajo, T.; Hirata, H.; Ono, M.; Utsumi, H. In vivo oxygen radical generation in the skin of the protoporphyria model mouse with visible light exposure: An L-band ESR study. *Journal of Investigative Dermatology* **122:**1463-1470; 2004.

[15]   Gutteridge, J. M. C.; Halliwell, B. Antioxidants: Molecules, medicines, and myths. *Biochemical and Biophysical Research Communications* **393:**561-564; 2010.

[16]   Gutteridge, J. M. C.; Halliwell, B. Free radicals and antioxidants in the year 2000 - A historical look to the future. *Annals of the New York Academy of Sciences* **899:**136-147; 2000.

[17]   Wu, T. Y.; Rifai, N.; Roberts, L. J.; Willett, W. C.; Rimm, E. B. Stability of measurements of biomarkers of oxidative stress in blood over 36 hours. *Cancer Epidemiology Biomarkers & Prevention* **13:**1399-1402; 2004.

[18]   Gutteridge, J. M. C. Lipid-Peroxidation and Antioxidants as Biomarkers of Tissue-Damage. *Clinical Chemistry* **41:**1819-1828; 1995.

[19]   Russell, G. A. Deuterium-isotope Effects in the Autoxidation of Aralkyl Hydrocarbons. Mechanism of the Interaction of Peroxy Radicals. *Journal of the American Chemical Society* **79:**3871-3877; 1957.

[20]   Ahmad, R.; Tripathi, A. K.; Tripath, P.; Singh, S.; Singh, R.; Singh, R. K. Malondialdehyde and protein carbonyl as biomarkers for oxidative stress and disease progression in patients with chronic myeloid leukemia. *In Vivo* **22:**525-528; 2008.

[21]   Dean, R. T.; Fu, S. L.; Stocker, R.; Davies, M. J. Biochemistry and pathology of radical-mediated protein oxidation. *Biochemical Journal* **324:**1-18; 1997.

[22]   Miyamoto, S.; Ronsein, G. E.; Prado, F. M.; Uemi, M.; Correa, T. C.; Toma, I. N.; Bertolucci, A.; Oliveira, M. C. B.; Motta, F. D.; Medeiros, M. H. G.; Di Mascio, P. Biological hydroperoxides and singlet molecular oxygen generation. *Iubmb Life* **59:**322-331; 2007.

[23]   Von Sonntag, C. *The chemical basis of radiation biology.* London: Taylor and Francis; 1987.

[24]   Pogozelski, W. K.; Tullius, T. D. Oxidative strand scission of nucleic acids: Routes initiated by hydrogen abstraction from the sugar moiety. *Chemical Reviews* **98:**1089-1107; 1998.

[25]   Prado, F. M.; Oliveira, M. C. B.; Miyamoto, S.; Martinez, G. R.; Medeiros, M. H. G.; Ronsein, G. E.; Di Mascio, P. Thymine hydroperoxide as a potential source of singlet molecular oxygen in DNA. *Free Radical Biology and Medicine* **47:**401-409; 2009.

[26]   Greer, A.; Vassilikogiannakis, G.; Lee, K. C.; Koffas, T. S.; Nahm, K.; Foote, C. S. Reaction of singlet oxygen with trans-4-propenylanisole. Formation of 2+2 products with added acid. *J. Org. Chem.* **65:**6876-6878; 2000.

[27]   Fedorova, G. F.; Trofimov, A. V.; Vasil'ev, R. F.; Veprintsev, T. L. Peroxy-radical-mediated chemiluminescence: mechanistic diversity and fundamentals for antioxidant assay. *Archive for Organic Chemistry:*163-215; 2007.

[28]   Uemi, M.; Ronsein, G. E.; Miyamoto, S.; Medeiros, M. H. G.; Di Mascio, P. Generation of Cholesterol Carboxyaldehyde by the Reaction of Singlet Molecular Oxygen O-2 ((1)Delta(g)) as Well as Ozone with Cholesterol. *Chemical Research in Toxicology* **22:**875-884; 2009.

[29]   Mano, C. M.; Prado, F. M.; Massari, J.; Ronsein, G. E.; Martinez, G. R.; Miyamoto, S.; Cadet, J.; Sies, H.; Medeiros, M. H. G.; Bechara, E. J. H.; Di Mascio, P. Excited singlet molecular O-2 ((1)Delta g) is generated enzymatically from excited carbonyls in the dark. *Scientific Reports* **4**; 2014.

[30]   Clennan, E. L. New mechanistic and synthetic aspects of singlet oxygen chemistry. *Tetrahedron Letters* **56:**9151-9179; 2000.

[31]   Adam, W.; Bosio, S. G.; Turro, N. J. Highly diastereoselective dioxetane formation in the photooxygenation of enecarbamates with an oxazolidinone chiral auxiliary: Steric control in the 2+2 cycloaddition of singlet oxygen through conformational alignment. *Journal of the American Chemical Society* **124:**8814-8815; 2002.

[32]   Corey, E. J.; Wang, Z. Conversion of arachidonic acid to the prostaglandin endoperoxide PGG(2), a chemical analog of the biosynthetic-pathway. *Tetrahedron Letters* **35:**539-542; 1994.

[33]   Cilento, G. Excited electronic states in dark biological processes. *Quarterly Reviews of Biophysics* **6:**485-501; 1974.

[34]   Bechara, E. J. H.; Oliveira, O.; Duran, N.; Debaptista, R. C.; Cilento, G. Peroxidase catalyzed generation of triplet acetone. *Photochemistry and Photobiology* **30:**101-110; 1979.

[35]   Turro, N. J.; Lechtken, P. Biacetyl sensitized decomposition of tetramethyl-1,2-dioxetane - example of anti-Stokes sensitization involving a masked excited state. *Tetrahedron Letters:*565-568; 1973.

[36]   Richardson, W. H.; Anderegg, J. H.; Price, M. E.; Tappen, W. A.; Oneal, H. E. Kinetics and mechanisms of thermal decomposition of triphenyl-1,1,2-dioxetane. *Journal of Organic Chemistry* **43:**2236-2242; 1978.

[37]   Baumstark, A. L.; Anderson, S. L.; Sapp, C. J.; Vasquez, P. C. Thermolysis of 3-alkyl-3-methyl-1,2-dioxetanes: Activation parameters and chemiexcitation yields. *Heteroatom Chemistry* **12:**176-179; 2001.

[38]   Miyamoto, S.; Rettori, D.; Augusto, O.; Martinez, G. R.; Medeiros, M. H. G.; Di Mascio, P. Linoleic acid hydroperoxide reacts with hypochlorite generating peroxyl radical intermediates and singlet oxygen. *Free Radical Biology and Medicine* **37:**S16-S16; 2004.

[39]   Hall, R.; Chamulitrat, W.; Takahashi, N.; Chignell, C.; Mason, R. Detection of Singlet oxygem phosphorescence during chloroperoxidase-catalyzed decomposition of ethyl hydroperoxide. *Journal of Biological Chemistry* **264:**7900-7906; 1989.

[40]   Howard, J. A.; Ingold, K. U. Absolute rate constants for hydrocarbon autooxidation .V. Hydroperoxy radical in chain propagation and termination. *Canadian Journal of Chemistry* **45:**785-&; 1967.

[41]   Adam, W.; Cilento, G. *Chemical and biological generation of excited states.* New York: Academic Press; 1982.

[42]   Cilento, G.; Nascimento, A. Generation of electronically excited triplet species at the cellular level: a potential source of genotoxicity. *Toxicology Letters* **67:**17-28; 1993.

[43]   Cilento, G.; Adam, W. From free radicals to electronically excited species. *Free Radical Biology and Medicine* **19:**103-114; 1995.

[44]   Boveris, A.; Cadenas, E.; Reiter, R.; Filipkowski, M.; Nakase, Y.; Chance, B. Organ chemi-luminescence - non-invasive assay for oxidative radical reactions. *Proceedings of the National Academy of Sciences of the United States of America-Biological Sciences* **77:**347-351; 1980.

[45]   Bennett, M.; Mehta, M.; Grant, M. Biophoton imaging: A nondestructive method for assaying R gene responses. *Molecular Plant-Microbe Interactions* **18:**95-102; 2005.

[46]   Darmanyan, A. P.; Foote, C. S. Solvent effects on singlet oxygen yield from N,PI-asterisk and PI,PI-asterisk triplet carbonyl compounds. *J. Phys. Chem.* **97:**5032-5035; 1993.

[47]   Mansfield, J. W. Biophoton distress flares signal the onset of the hypersensitive reaction. *Trends in Plant Science* **10:**307-309; 2005.

[48]   Niu, E. P.; Mau, A. W. H.; Ghiggino, K. P. Dye-sensitized photooxidation of anthracene and its derivatives in nafion membrane. *Australian Journal of Chemistry* **44:**695-704; 1991.

[49]   Niu, Q. J.; Mendenhall, G. D. Yields of singlet molecular oxygen from peroxyl radical termination. *Journal of the American Chemical Society* **114:**165-172; 1992.

[50]   Kanofsky, J. R. Singlet oxygen production from the peroxidase catalyzed formation of styrene glutathione adducts. *Biochemical and Biophysical Research Communications* **159:**1051-1054; 1989.

[51]   Pospíšil, P.; Prasad, A.; Rác, M. Role of reactive oxygen species in ultra-weak photon emission in biological systems. *Journal of Photochemistry and Photobiology B: Biology*; 2014.

[52]   Cadenas, E.; Arad, I. D.; Boveris, A.; Fisher, A. B.; Chance, B. Partial spectral-analysis of the hydroperoxide-induced chemi-luminescence of the perfused lung. *Febs Letters* **111:**413-418; 1980.

[53]   Cadenas, E.; Boveris, A.; Chance, B. Spectral analysis of the low level chemiluminescence of H2O2-supplemented ferricytochrome c. *Febs Letters* **112:**285-289; 1980.

[54]   Van Wijk, R.; Kobayashi, M.; Van Wijk, E. P. A. Spatial characterization of human ultra-weak photon emission. *Biophotonics and Coherent Systems in Biology***:**177-189; 2007.

[55]   Cadenas, E.; Arad, I. D.; Fisher, A. B.; Boveris, A.; Chance, B. Hydroperoxide-induced chemiluminescence of the perfused lung. *Biochemical Journal* **192:**303-309; 1980.

[56]   Cadenas, E.; Varsavsky, A. I.; Boveris, A.; Chance, B. Oxygen- or organic hydroperoxide-induced chemiluminescence of brain and liver homogenates. *Biochemical Journal* **198:**645-654; 1981.

[57]   Hideg, E.; Kobayashi, M.; Inaba, H. Spontaneous Ultraweak Light-Emission from Respiring Spinach Leaf Mitochondria. *Biochim Biophys Acta* **1098:**27-31; 1991.

[58]   Mathew, B. G.; Roy, D. Weak luminescence from the frozen-thawed root tips of Cicer arietinum. L. *Journal of Photochemistry and Photobiology B-Biology* **12:**141-150; 1992.

[59]   Agatsuma, S.; Nagoshi, T.; Kobayashi, M.; Usa, M.; Watanabe, H.; Sekino, H.; Inaba, H. Hydroxyl radical-induced characteristics chemiluminescent spectra from plasma of hemodyalysis-patients. *Clinical Chemistry* **38:**48-55; 1992.

[60]   Ma, W.; Cao, E.-H.; Zhang, J.; Qin, J.-F. Phenanthroline-Cu complex-mediated chemiluminescence of DNA and its potential use in antioxidation evaluation. *Journal of Photochemistry and Photobiology B: Biology* **44:**63-68; 1998.

[61]   Takeda, M.; Tanno, Y.; Kobayashi, M.; Usa, M.; Ohuchi, N.; Satomi, S.; Inaba, H. A novel method of assessing carcinoma cell proliferation by biophoton emission. *Cancer Letters* **127:**155-160; 1998.

[62]   Kageyama, C.; Kato, K.; Iyozumi, H.; Inagaki, H.; Yamaguchi, A.; Furuse, K.; Baba, K. Photon emissions from rice cells elicited by N-acetylchitooligosaccharide are generated through phospholipid signaling in close association with the production of reactive oxygen species. *Plant Physiology and Biochemistry* **44:**901-909; 2006.

[63]   Khabiri, F.; Hagens, R.; Smuda, C.; Soltau, A.; Schreiner, V.; Wenck, H.; Wittern, K.-P.; Duchstein, H.-J.; Mei, W. Non-invasive monitoring of oxidative skin stress by ultraweak photon

emission (UPE)-measurement. I: mechanisms of UPE of biological materials. *Skin Research and Technology* **14:**103-111; 2008.

[64]   Cadenas, E.; Boveris, A.; Chance, B. Low-level chemiluminescence of hydroperoxide-supplemented cytochrome c. *Biochemical Journal* **187:**131-140; 1980.

[65]   Mathew, B. G.; Haorah, J.; Kumar, S. Weak Luminescence from Cotyledons of Cicer-Arietinum L Induced by Sudden Freezing and Thawing - the Role of Superoxide, Free-Radicals and Singlet Oxygen in the Phenomenon. *Journal of Photochemistry and Photobiology B-Biology* **16:**297-304; 1992.

[66]   Miyamoto, S.; Martinez, G. R.; Rettori, D.; Augusto, O.; Medeiros, M. H. G.; Di Mascio, P. Linoleic acid hydroperoxide reacts with hypochlorous acid, generating peroxyl radical intermediates and singlet molecular oxygen. *Proceedings of the National Academy of Sciences of the United States of America* **103:**293-298; 2006.

[67]   Pilz, J.; Meineke, I.; Gleiter, C. H. Measurement of free and bound malondialdehyde in plasma by high-performance liquid chromatography as the 2,4-dinitrophenylhydrazine derivative. *Journal of Chromatography B* **742:**315-325; 2000.

[68]   Pou, T. E.; Murphy, O. J.; Young, V.; Bockris, J. O.; Tongson, L. L. Passive films on iron - the mechanism of breakdown in chloride containing solutions. *Journal of the Electrochemical Society* **131:**1243-1251; 1984.

[69]   Moan, J.; Wold, E. Detection of singlet oxygen production by ESR. *Nature* **279:**450-451; 1979.

[70]   Wei, S. H.; Zhou, J. H.; Huang, D. Y.; Wang, X. S.; Zhang, B. W.; Shen, J. Synthesis and Type I/Type II photosensitizing properties of a novel amphiphilic zinc phthalocyanine. *Dyes and Pigments* **71:**61-67; 2006.

[71]   Gollmer, A.; Arnbjerg, J.; Blaikie, F. H.; Pedersen, B. W.; Breitenbach, T.; Daasbjerg, K.; Glasius, M.; Ogilby, P. R. Singlet Oxygen Sensor Green (R): Photochemical Behavior in Solution and in a Mammalian Cell. *Photochemistry and Photobiology* **87:**671-679; 2011.

[72]   Shen, Y.; Lin, H. Y.; Huang, Z. F.; Chen, D. F.; Li, B. H.; Xie, S. S. Indirect imaging of singlet oxygen generation from a single cell. *Laser Physics Letters* **8:**232-238; 2011.

[73]   Repetto, M. G.; Ferrarotti, N. F.; Boveris, A. The involvement of transition metal ions on iron-dependent lipid peroxidation. *Archives of Toxicology* **84:**255-262; 2010.

[74]   Halliwell, B.; Chirico, S. Lipid-peroxidation - its mechanism, measurement, and significance. *American Journal of Clinical Nutrition* **57:**S715-S725; 1993.

[75]   Russell, G. A. Deuterium-Isotope Effects in the Autoxidation of Aralkyl Hydrocarbons - Mechanism of the Interaction of Peroxy Radicals. *J. Am. Chem. Soc.* **79:**3871-3877; 1957.

[76]   Berlett, B. S.; Stadtman, E. R. Protein oxidation in aging, disease, and oxidative stress. *Journal of Biological Chemistry* **272:**20313-20316; 1997.

[77]   Dean, R. T.; Gieseg, S.; Davies, M. J. Reactive species and their accumulation on radical-damaged proteins. *Trends in Biochemical Sciences* **18:**437-441; 1993.

[78]   Tweeddale, H. J.; Kondo, M.; Gebicki, J. M. Proteins protect lipid membranes from oxidation by thiyl radicals. *Archives of Biochemistry and Biophysics* **459:**151-158; 2007.

[79]   Du, J.; Gebicki, J. M. Proteins are major initial cell targets of hydroxyl free radicals. *International Journal of Biochemistry & Cell Biology* **36:**2334-2343; 2004.

[80]   Tweeddale, H.; Gebicki, J. M. Effect of proteins and amino acids on oxidation of liposomes by hydroxyl and peroxyl free radicals. *Redox Report* **7:**332-334; 2002.

[81]   Gieseg, S.; Duggan, S.; Gebicki, J. M. Peroxidation of proteins before lipids in U937 cells exposed to peroxyl radicals. *Biochemical Journal* **350:**215-218; 2000.

[82]   Simpson, J. A.; Narita, S.; Gieseg, S.; Gebicki, S.; Gebicki, J. M.; Dean, R. T. Long-lived reactive species on free-radical-damaged proteins. *Biochemical Journal* **282:**621-624; 1992.

[83]   Minisini, M. P.; Kantengwa, S.; Polla, B. S. DNA-damage and stress protein-synthesis induced by oxidative stress proceed independently in the human premonocytic line U937. *Mutation Research-DNA Repair* **315:**169-179; 1994.

[84]   Sagripanti, J. L.; Kraemer, K. H. Site-specific oxidative DNA damage at polyguanosines produced by copper plus hydrogen peroxide. *Journal of Biological Chemistry* **264:**1729-1734; 1989.

[85]   Wiseman, H.; Halliwell, B. Damage to DNA by reactive oxygen and nitrogen species: Role in inflammatory disease and progression to cancer. *Biochemical Journal* **313:**17-29; 1996.

[86]   Cadet, J.; Wagner, J. R. DNA Base Damage by Reactive Oxygen Species, Oxidizing Agents, and UV Radiation. *Cold Spring Harbor Perspectives in Biology* **5**; 2013.

[87]   Cadenas, E.; Boveris, A.; Chance, B. Spectral analysis of the low level chemiluminescence of H2O2-supplemented ferricytochrome c. *FEBS Lett.* **112:**285-288; 1980.

[88]   Mathew, B. G.; Haorah, J.; Kumar, S. Weak Luminescence from Cotyledons of Cicer-Arietinum L Induced by Sudden Freezing and Thawing - the Role of Superoxide, Free-Radicals and Singlet Oxygen in the Phenomenon. *J Photoch Photobio B* **16:**297-304; 1992.

[89]   Timmins, G. S.; dosSantos, R. E.; Whitwood, A. C.; Catalani, L. H.; Di Mascio, P.; Gilbert, B. C.; Bechara, E. J. H. Lipid peroxidation-dependent chemiluminescence from the cyclization of alkylperoxyl radicals to dioxetane radical intermediates. *Chemical Research in Toxicology* **10:**1090-1096; 1997.

[90]   Miyamoto, S.; Martinez, G. R.; Medeiros, M. H. G.; Di Mascio, P. Singlet molecular oxygen generated by biological hydroperoxides. *Journal of Photochemistry and Photobiology B: Biology*; 2014.

[91]   Sun, S.; Bao, Z.; Ma, H.; Zhang, D.; Zheng, X. Singlet oxygen generation from the decomposition of alpha-linolenic acid hydroperoxide by cytochrome c and lactoperoxidase. *Biochemistry* **46:**6668-6673; 2007.

Publications